CODEN:LUTEDX/(TEIE-5406)/1-112(2018)

Industrial Electrical Engineering and Automation

New Principle for Fluid Flow Measurement

Markus Karlström
Fredrik Olsson

Division of Industrial Electrical Engineering and Automation
Faculty of Engineering, Lund University

LUNDS UNIVERSITET

MASTER THESIS

New Principle for Fluid Flow Measurement

Authors:
Markus KARLSTRÖM
Fredrik OLSSON

Supervisor:
Sebastian HALL

Assistant Supervisor:
Michael PETTERSSON

Examiner:
Gunnar LINDSTEDT

A thesis submitted in fulfilment of the requirements for the degree of Master of Science in engineering

at the department of

Industrial Electrical Engineering and Automation
Lunds Tekniska Högskola

May 31, 2018

Declaration of Authorship

We, Markus KARLSTRÖM & Fredrik OLSSON, declare that this thesis titled, "New Principle for Fluid Flow Measurement" and the work presented in it are our own. We confirm that:

- This work was done wholly or mainly while in candidature for a masters degree at this University.
- Where any part of this thesis has previously been submitted for a degree or any other qualification at this University or any other institution, this has been clearly stated.
- Where we have consulted the published work of others, this is always clearly attributed.
- Where we have quoted from the work of others, the source is always given. With the exception of such quotations, this thesis is entirely our own work.
- We have acknowledged all main sources of help.
- Where the thesis is based on work done by ourselves jointly with others, We have made clear exactly what was done by others and what we have contributed ourselves.
- We have divided the work equally between us.

Signed: Date:

Markus KARLSTRÖM

Signed: Date:

Fredrik OLSSON

"Debugging is twice as hard as writing the code in the first place. Therefore, if you write the code as cleverly as possible, you are, by definition, not smart enough to debug it."

Brian Kernighan

LUNDS UNIVERSITET

Abstract

Lunds Tekniska Högskola
Industrial Electrical Engineering and Automation

Master of Science in engineering

New Principle for Fluid Flow Measurement

by Markus KARLSTRÖM & Fredrik OLSSON

Fluid flow measurement is a task for which many different solutions exist. For high precision sensors the production cost is high and measurement principle is generally based on advanced theory. In this thesis a new principle of fluid flow measurement, based on the concept of a conventional rotameter, is investigated. The new principle uses a solenoid to create a magnetic field to maintain a float, placed in the flow path, at a fixed position. A model is then created to approximate the relation between fluid flow and the current in the solenoid.

The principle is, in this thesis, verified as a possible method of measuring fluid flow. A number of properties and disturbances (i.e. pressure, temperature, tilt and air bubbles) are investigated as to see how they affect the measurement principle. In all cases an observable effect has been identified. Most disturbances i.e. pressure, tilt and air bubbles are assumed to be possible to avoid or remove. It is, however, found that there is a need to include a temperature compensation in the model.

The new principle is seen as a promising method of measuring fluid flow with simple tools and low costs of manufacturing. There is a need to test the effect of additional parameters and disturbances to verify the reliability of the principle.

Keywords: flow measurement, rotameter, solenoid, magnet, drag

Sammanfattning

Det finns idag många olika lösningar för att mäta fluidflöden. För att uppnå hög precision i mätningarna blir sensorernas tillverkningskostnad ofta hög och deras principer är generellt baserade på avancerad teori. I det här examensarbetet undersöks en ny mätprincip, baserad på konceptet för en vanlig rotameter. Den nya mätprincipen använder en solenoid för att skapa ett magnetiskt fält som håller en svävkropp, placerad i flödesbanan, i en fix position. En modell skapas utifrån förhållandet mellan vätskeflödets magnitud och strömstyrkan i solenoiden.

I det här examensarbetet verifieras metoden som ett möjligt sätt att mäta vätskeflöde. Ett antal parametrar och störningar (mer bestämt tryck, temperatur, lutning och luftbubblor) undersöks för att se hur de påverkar mätprincipen. För samtliga av dessa fyra har en påverkan kunnat observeras. För de flesta störningarna, tryck, lutning och introduktion av luftbubblor, anses det finnas möjlighet att minska eller undvika mätfel. När det kommer till temperaturparametern anses det finnas ett behov av att ta med en temperaturmätning i skapandet av flödesmätningens modell.

Den nya principen anses vara en lovande metod för att mäta flöde med enkla verktyg och låga tillverkningskostnader. Det finns ett behov av vidare testning av andra parameterar och störningars påverkan på systemet. Med omfattande testning, av parametrarna testade i det här arbetet, samt tillägg av andra relevanta parametrar, kan tillförlitligheten i den nya principen fastställas.

Nyckelord: flödesmätning, rotameter, solenoid, magnet, strömningsmotstånd

Preface and Acknowledgements

This thesis is performed to fulfil the requirements of graduation of the Mechanical Engineering program at LTH. The thesis was written between January and June 2018.

The thesis is written on request of Baxter Lund and a big thank you is owed to all Baxter employees who have helped us during our time there.

A special thank you to Michael Petterson, our supervisor, who has been a great source of help, support and guidance.

Also, a special thank you to Måns Fällman, our extra source of help in all problems, big and small.

Thank you, to the other innovators behind this idea, Daniel Ståhl and Sven Gustafson, who assisted with their expertise.

Thank you, Sebastian Hall, for great guidance through the jungle of academic writing as well as all support and help along the way.

Thank you, Gunnar Lindstedt, for helping with administration and always keeping an open door.

Markus KARLSTRÖM & Fredrik OLSSON

Contents

Glossary

hemodialysis	a dialysis treatment that uses a machine to treat a patient's blood through exchange over a filter
peritoneal dialysis	a dialysis treatment using the peritoneum as a filter instead of a manufactured one
hypervolemia	a condition of too much fluid in the blood
ultrafiltration	fluid transport past a semi permeable membrane driven by a pressure difference over the membrane
rotameter	an instrument used for measuring flow
buoyancy	lifting force caused by a fluid on an immersed body
annulus	a ring shaped area defined by an inner and an outer diameter

1 Introduction

This chapter presents the background for this thesis along with the purpose and scope. The chapter also includes a short description of methods used and the general work flow.

1.1 Background

Patients who suffer from renal failure need to be treated with e.g. dialysis to regulate the patient's hemodynamic levels as their kidneys can not. This can mainly be done by either of two methods: hemodialysis (HD) and peritoneal dialysis (PD). Hemodialysis is a treatment where the properties of the patient's blood (e.g. fluid balance, electrolytes and toxin concentrations) are controlled in an extracoporeal blood circuit. The machine removes toxins, excessive fluid and corrects the acid-base balance.

Hemodialysis is performed with three different goals. The primary is to remove excessive fluid from the body to prevent hypervolemia. This process is called *ultrafiltration*. Furthermore, the dialysis serves to regulate the electrolyte concentrations in the blood. To control this process, the blood of the patient is driven past a semi-permeable membrane in a dialysis filter with a dialysis fluid on the other side of the membrane. During the process of the hemodialysis, the salinity and other concentrations in the blood converge to the ones of the dialysis fluid. At the same time, a pressure difference over the membrane drives the process of ultrafiltration. The third goal is to control the temperature of the blood which is desired to be about $37^{\circ}C$ to avoid chilling the patient.

For the ultrafiltration, the measurement of the fluid flow rate is critical. The difference between the flow into and out from the machine needs to be measured with high accuracy. As the treatment is performed for several hours, a small error in the measurement can result in too large amounts of fluid being removed from the patient or it could result in fluids being added. The consequences can in both cases be severe and even fatal.

Flow measurement with high accuracy and precision is today complex and the sensors are expensive to manufacture and to calibrate. The current method of fluid flow measurement is old and the devices are bigger than desired. Therefore, there is a need to improve the current methods of flow measurement or to find new alternatives [1].

This thesis is performed on request of Baxter, Lund. Baxter is a global company which creates healthcare products. Their products can be found in hospitals and homes, all around the world. In Lund, Baxter develops and produces hemodialysis machines. In short, the goal is to design a fluid flow rate sensor based on a new principle of measurement. The principle was determined before the start of the project and the purpose of the project is to both verify that the principle works as well as design a working fluid flow sensor.

1.2 Purpose & Principle

The purpose of this thesis is to investigate the possibility to design a fluid flow sensor that is simple, small and has a low total manufacturing cost. More precisely, to use the simple concept of the conventional rotameter, and modify it to make it possible to read the measurement with an electric signal. This has been done in [2] and [3], but not quite in the same manner.

1.2.1 Conventional Rotameter Principle

The new principle of measurement that is to be investigated and verified in this thesis is partly based on the principle of a rotameter. Therefore the basics of a rotameter are explained. Rotameters operate by a vertically placed, tapered tube with a float inside. As the tube is tapered, the cross-sectional area varies as the float changes its vertical position. Therefore, different vertical positions of the float correspond to different velocities in the fluid around it. A given flow rate affects the float with a certain drag force caused by both the frictional force and the pressure drop over it. If the drag force is larger than the resultant force of gravity and buoyancy, the float rises until the velocity decreases and a force equilibrium is achieved. If the flow rate decreases, gravity forces the float down to equilibrium at a lower position. From equations about rotameters like those presented in [4] a graded scale can be placed along the tapered tube to let the floats position indicate different flow rates. A figure of the forces acting on a float in a rotameter is shown in figure 1.1.

Rotameters are commonly used to determine the fluid flow rate visually. That is, the float moves along a graded scale where the user can look at the floats position and read the current flow rate from the scale. The advantages of the conventional rotameter is that it is simple and has a low production cost. On the other hand, it is not very precise and does not transmit an electrical measurement signal.

1.2.2 New Principle of Measurement

The new principle takes the idea of the rotameter but uses a straight tube instead of a tapered. With a straight tube, there is only one flow rate that achieves force equilibrium. The "position of equilibrium" can therefore be any position in the tube. Flows below the equilibrium flow rate makes the float move downwards and flows above causes the float to rise. This connects the flow rate directly to the resulting force affecting the float.

To balance out the drag force, an extra force is added so that the float can be positioned in a fixed position, independent of the flow rate. The new principle uses the magnetic force from a solenoid around the tube, as the extra force. For the float to be affected by the solenoid, it needs to be magnetic. An electric current, I, controls the magnetic force, F_m, as $F_m \propto I$. While keeping the float in a fixed position, the current controlling the solenoid can be measured. The idea is to find the relation between different currents in the solenoid and corresponding flow rates in the tube. In figure 1.2 the new principle is illustrated.

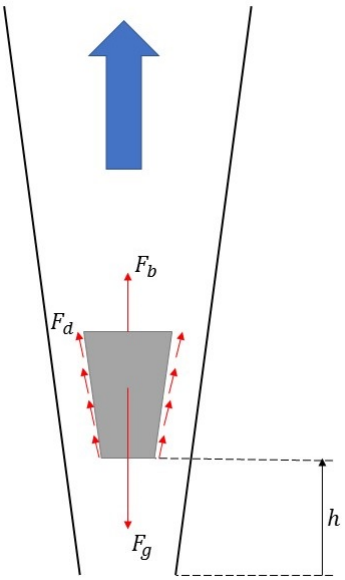

FIGURE 1.1: Principle of a rotameter. F_b is buoyancy force, F_g is force of gravity and F_d is drag force.

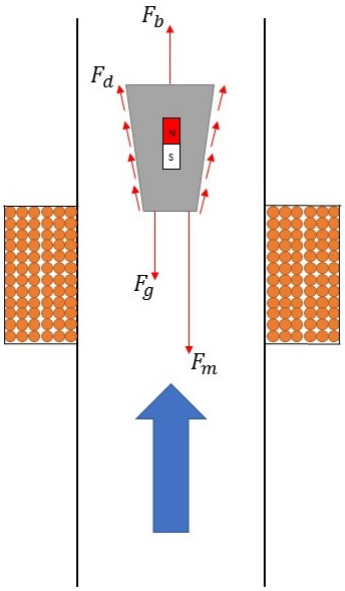

FIGURE 1.2: Principle of the new principle. F_m is the added magnetic force.

1.2.3 Scope

To set the scope for the thesis the conditions for the proposed application, in an HD machine, is considered. The boundaries of the investigated flow rates are set according to the range of flow rates in Baxter's HD machines. Since the goal of dialysis is to alter the properties of the fluids, effects of different fluid properties and compositions are relevant to analyse. Testing the accuracy and precision is of also of interest. The scope of the thesis is compiled to the following:

- Is it possible to measure a fluid flow in the range of 0.3 l/min to 0.8 l/min with the new principle?
- Given that the new principle is verified, how good is the accuracy and precision of the sensor?
- How good is the accuracy and precision of the measurement at different flow rates?
- Will changes in temperature and pressure of the fluid affect the measurement?
- How does the new principle handle air disturbances and a tilted orientation?
- Do the test results agree with the underlying theory?

1.3 Method

The approach of this thesis will be a division of the problem into several sub problems. This is seen as a relevant approach as there are various parts to design and build that cover different disciplines. To have a better understanding of how the problem division is made, a number of milestones are set up.

1.3.1 Milestones

The milestones of the thesis include the disciplines of engineering work, fluid dynamics, electromagnetism, programming, control and statistical verification. The milestones of the thesis are set to be the following:

1. *Setting up the test-rig*, and verify its sensors and actuators. Construct a reliable control system to run tests.
2. *Design a float* that behaves well within the specified flow range.
3. *Design a solenoid* which can control a magnetic float well within the specified flow range.
4. *Development of control software* which can keep a steady flow and current in the system.
5. *Ability to control the float* to maintain a fixed position at different flow rates.
6. *Mapping* of the relation between electric current in the solenoid and the fluid flow rate.
7. *List and analyse* the different effects of properties such as temperature, pressure, tilt and air disturbance.

1.4 Thesis structure

The content of the thesis will be divided in the following chapters and presented in that order:

- Theory: The theory considered in the design stages and on which the analyses are based.
- Sensor Design: A presentation of design choices, and functional tests.
- Test Rig: A description of the material used for conducting the tests.
- Sensor Evaluation: A presentation and analysis of the conducted tests and results.
- Discussion and Future Prospects: Discussion of the gathered results and what the future of the sensor might be.
- Conclusion: A summary of the most important points of the thesis.

2 Theory

The new principle consist of four forces, *gravity*, *buoyancy*, *drag* and *magnetism*. Theory regarding these forces is presented in this chapter.

2.1 The New Principle

The new principle is based on achieving a force equilibrium between four forces in the direction of the flow. The float is affected by the gravity, buoyancy, drag force and magnetic force. Equation (2.1) needs to be fulfilled for the float to be at rest.

$$F_g + F_b + F_d + F_m = 0 \tag{2.1}$$

Where F_g is the force of gravity, F_b is force from buoyancy, F_d is drag force from the fluid flow, F_m is magnetic force between the solenoid and the magnetic float.

For the force equation to be fulfilled the magnetic force needs to increase when the drag force increase. In order to increase the magnetic force, the electrical current needs to increase. This is the basics for the new principle. The force of gravity and the buoyancy remains constant in a system when no properties changes.

2.2 Gravity

The force of gravity is constant in a stable system, and is determined by Equation (2.2).

$$F_g = mg\cos\theta \tag{2.2}$$

Where m is the mass of the float, g is the gravitational acceleration and θ is the angle of the sensor in relation to a vertical axis, see Figure 2.1. In a stable system, the force of gravity is constant, since the mass and acceleration remains constant. If the sensor is tilted the gravitational force component against the fluid flow decreases.

2.3 Buoyancy

The force due to buoyancy is determined from Archimedes' principle, as shown in simplified form in Equation (2.3).

$$F_b = \rho_{fluid} g V \cos\theta \tag{2.3}$$

Where ρ_{fluid} is the density of the fluid, V is the volume of the float, θ is the same angle as in Equation (2.2) and g still represents gravity.

Gravity is constant and the volume of the float is assumed to remain constant throughout all temperature changes. In a stable system this force is therefore constant. However, the density of the fluid in the system can change due to changes in temperature or composition of the fluid. This affects the buoyancy force. Just as in the case of the gravity force, the buoyancy force component also changes with the angle θ when the sensor is tilted.

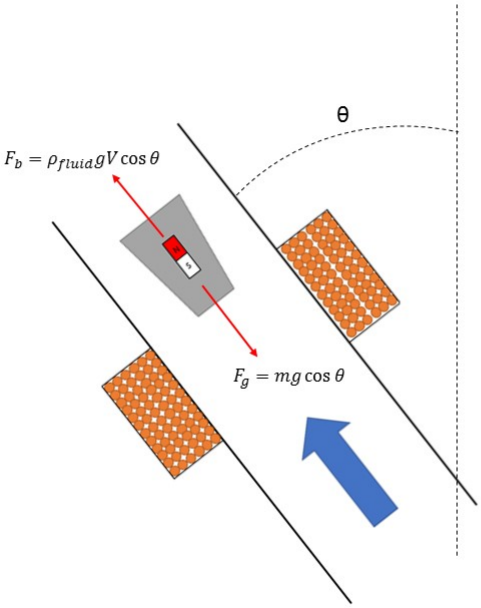

FIGURE 2.1: Illustration of gravity and buoyancy relation to θ

2.4 Drag

Fluid dynamics are mostly investigated by using CFD or experimental data, since there does not exist a general analysis of flow yet [5]. In the following sections theory regarding internal flow and external flow past immersed bodies are explained separately. The new principle is similar to a rotameter, which is well studied. Theory of rotameter is presented, to see which parameters it is affected by.

2.4.1 Internal Flow Theory

Internal flow is that is bounded by surrounding walls e.g. flow in a tube. Flow can either be laminar or turbulent. In Figure 2.2 the two different characteristics are illustrated.

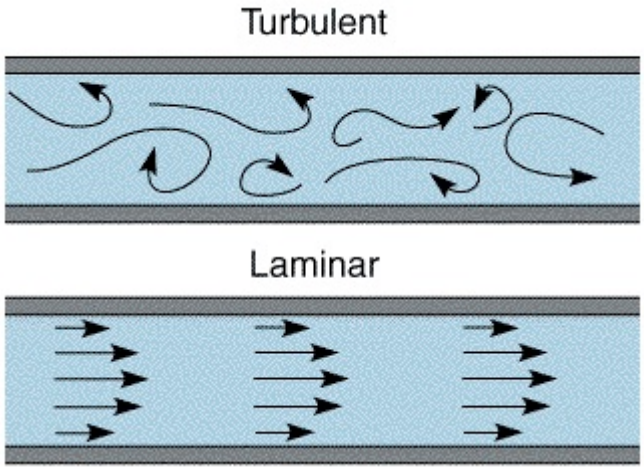

FIGURE 2.2: Illustration of turbulent and laminar flow. *Lucho, "Flujo-laminar-y-turbulento"* [6].

Laminar flow means that the flow is smooth and steady. While turbulent indicates that the flow is chaotic and not smooth. Between these two cases a transition area exists, this area depends on various factors but Reynolds number is the primary factor. Reynolds number, Re, in a tube is given by Equation (2.4)

$$Re = \frac{U \cdot d}{\nu} \tag{2.4}$$

where U is the fluid velocity, D is the diameter of the tube, and ν is the kinematic viscosity of the fluid. An approximated range for different Reynolds number are as follows:

$0 < Re < 10^3$ - Laminar

$10^3 < Re < 10^4$ - Transition from laminar to turbulent

$10^4 < Re < \infty$ - Turbulent

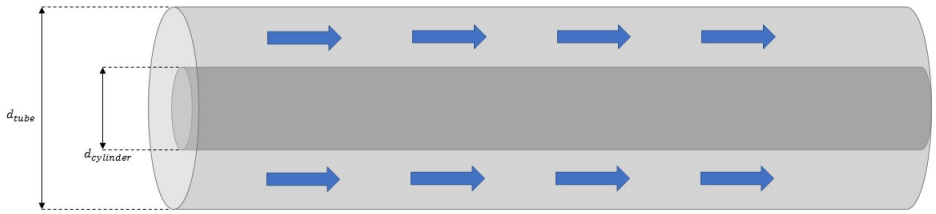

FIGURE 2.3: Illustration of a concentric annulus.

When a cylinder is placed inside a tube, forming a concentric annulus as in Figure 2.3, the velocity increases due to a smaller cross-sectional area which the fluid can pass through. The equation for Reynolds number is given by Equation (2.5), which is most accurate for long tubes and cylinders.

$$Re_d = \frac{U_h \cdot d_h}{\nu} \tag{2.5}$$

Reynolds number is then calculated using the hydraulic diameter d_h which is determined by $d_h = d_{tube} - d_{cylinder}$. The velocity U_h of the fluid in the annulus are given by Equation (2.6). The variable ν still represents the kinematic viscosity.

$$U_h = \frac{Q}{A_{tube} - A_{Cylinder}} \tag{2.6}$$

The velocity U_h is determined by the annulus area $A_{tube} - A_{Cylinder}$, where A_{tube} is the cross-sectional area of the tube and $A_{cylinder}$ is the cross-sectional area of the cylinder, and the fluid flow rate Q as in Equation (2.6) [5].

2.4.2 External Flow Past Immersed Bodies

External flow past immersed bodies is e.g. a sphere or any other arbitrary body placed within a stream. The flow is not constrained by surrounding walls.

An important parameter for the new principle is how much drag force the float is affected by from the fluid flow rate. The drag coefficient C_D is vital to determine the drag force since C_D is a factor in the drag force which generally is described as Equation (2.7).

$$F_d = C_D \frac{\rho U^2}{2} A \tag{2.7}$$

Where ρ is the density of the fluid and A is the cross section area of the float. The velocity of the fluid becomes zero at some point when the flow encounters the float. This point is called the stagnation point which occurs at the front of the float. At this point high static pressure occurs. At the end of the float wakes appears, which leads to a lower pressure. Also when the fluid is flowing over the body, the body is affected by shear stress. Therefore, the drag coefficient has contribution from both the *pressure drag* and from *friction drag*. Consequently, C_D becomes as in (2.8).

$$C_D = C_{D,press} + C_{D,fric} \tag{2.8}$$

In the same manner as Reynolds number describes the characteristics of internal flow it can be calculated for external flow past an immersed body. Reynolds number past an immersed body is given by (2.9).

$$Re = \frac{Ud}{\nu} \tag{2.9}$$

Where d is the diameter of the float, assumed a rotational symmetric float [5]. As in the earlier case, U is the fluid velocity and ν the fluid kinematic viscosity.

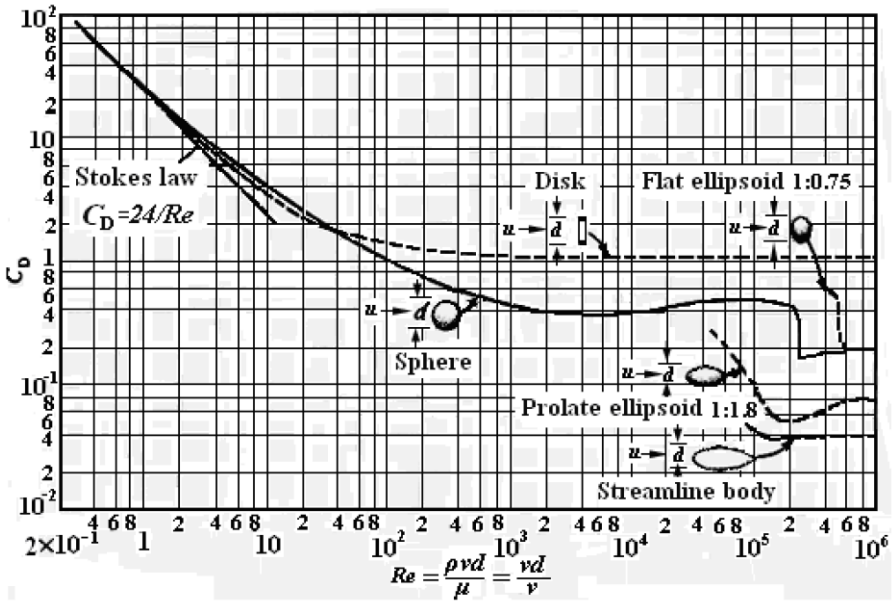

FIGURE 2.4: Relation between C_D and Reynolds number for some bodies.
X. B. Zhao, X. Zhou, "Engineering fluid mechanic" [7].

The drag coefficient is determined by Reynolds number, float shape, roughness of its surface, and the kinematic viscosity of the fluid. The drag coefficient can not be calculated theoretically, it is obtained by experiments. In Figure 2.4 it is seen how C_D changes due to Reynolds number for some different float shapes [4].

2.4.3 Rotameter

Theory for flow in a rotameter is well defined. According to [4] it is possible to describe the dynamics of fluid flow in a rotameter as the dynamics around an immersed body in external flow. Their equation for calculating the flow rate in a rotameter is given by (2.10).

$$Q = \frac{1}{\sqrt{C_D}}(A_{R0} + \pi h^2 \tan^2\theta + \pi h D_m \tan\theta)\sqrt{\frac{2gV_f(\rho_f - \rho)}{\rho A_f}} \tag{2.10}$$

Where A_{R0} is the narrowest area between the tube and the floats largest cross section when the float is at zero position in the rotameter, h is the height of the float relative to the zero position in the rotameter, θ is the angle of the tapered tube, D_m is the diameter of the tapered tube in the zero position, V_f is the volume of the float, ρ is the fluid density, ρ_f is the density of the float and A_f is the largest cross section of the float [4].

In Equation (2.10) some parameters are determined by the geometrical design, and remain fixed over time. In the new principle, the height h is also fixed. Therefore, is it possible to rewrite (2.10) to (2.11).

$$Q = \frac{1}{\sqrt{C_D}}(A_R)\left(\sqrt{\frac{2gV_f}{A_f}}\right)\sqrt{\frac{(\rho_f - \rho)}{\rho}} = D\frac{1}{\sqrt{C_D}}\sqrt{\frac{(\rho_f - \rho)}{\rho}} \tag{2.11}$$

Where D is a constant which is determined by the physical design and fixed variables, ρ_f is also constant. Equation (2.11) indicates that when fluid flows through a rotameter with fixed dimensions and a fixed height of the float, the parameters that can affect the flow measurement is C_D and ρ. Density as well as viscosity of water are temperature dependent. The variation of density and viscosity is plotted in Figure 2.5 [8].

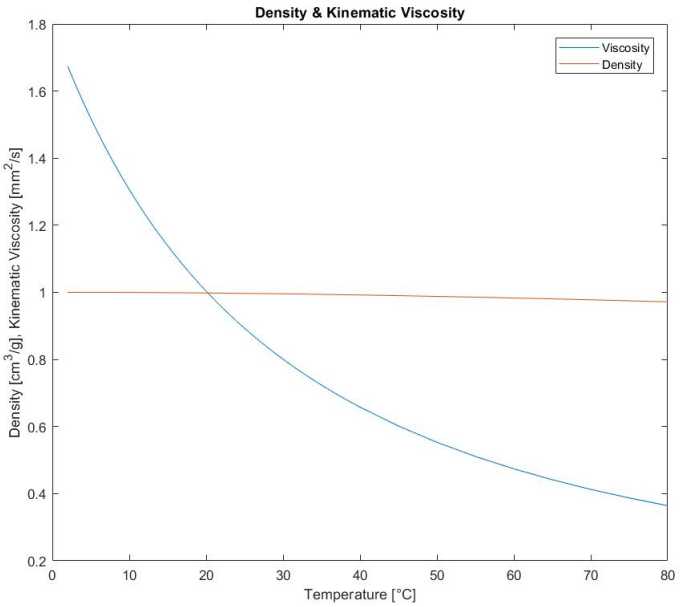

FIGURE 2.5: Plotted curves for the kinematic viscosity and density for water at specific temperatures.

2.4.4 Vital Parameters for the New Principle

This section combines theory from the previous sections and builds a theory about what parameters are vital in the new principle. A body immersed in external flow experiences both stagnation pressure and pressure from the wake, and a float in a tube experiences the same. The frictional factor of C_D also contributes to the drag force for a float within a tube [4].

Studying Equation (2.5), (2.6) and (2.7) it is seen that the drag force is dependent of the flow rate, diameter of tube and float, density of fluid and the drag coefficient. The drag coefficient is dependent of Reynolds number which also is affected by the kinematic viscosity of the fluid. The drag coefficient is also affected by the floats body shape and the roughness of its surface. To determine the drag force several parameters need to be considered which makes the drag force complex to theoretically calculate [5].

2.5 Magnetism

The magnitude of the magnetic force acting between the float and the solenoid is a combination of several parameters. The main parameters are the relative position and orientation of the objects, the strength of the magnetic float, and the strength of the magnetic field from the solenoid which is dependent on the current applied to the coil. The physical design of the solenoid affects which position the float operates in, and where position sensors are attached.

Theory for magnetic fields is complex. Therefore is it common practice that these forces are either found experimentally or calculated with finite element methods.

2.5.1 Magnetic float

To achieve a magnetic float one solution is to place a permanent magnet inside the float. Another solution is to use a piece of magnetic material e.g. iron.

Permanent magnets demagnetize over time and when exposed to high temperatures. Common industrial permanent magnets are neodymium magnets (NdFeB magnets). Neodymium magnets can lose 6 % of their magnetic polarisation over a time span of 30 years when exposed to room temperature. When the magnet is exposed to temperature over its critical temperature, losses in polarisation after 30 years can rise to 10 %. However, if the material for the magnet is well selected, it is possible to have almost no losses [9].

2.5.2 Magnetic Force

The magnetic force acting between a permanent magnet and a solenoid is complex to determine theoretically. Between a thin coil and a permanent magnet the magnetic force can be expressed as in Equation (2.12) [10].

$$F_m = \frac{J_1 J_2}{2\mu_0} \sum_{e_1,e_2}^{\{1,-1\}^2} e_1 e_2 m_1 m_2 m_3 f_s \tag{2.12}$$

Where J_1 and J_2 describe the strength of the two magnets. J_1 is a constant parameter of the permanent magnet and can be exchanged for the permanent magnet strength, B_r ('r' for radial). J_2 is the solenoid equivalent but is not constant. It is calculated as in (2.13). The variables m_1 m_2 and m_3 are determined by dimensions of the permanent magnet and the solenoid and f_s is an expression of m_1 m_2 and m_3. The variable m_1 also contains the distance between the permanent magnet and the solenoid, hence the force is dependent on the distance. The variables e_1 and e_2 are orthogonal directional vectors. The solenoid magnetic strength J_2 is given by (2.13).

$$J_2 = \frac{\mu_0 N_z I}{l} \tag{2.13}$$

Where μ_0 is the permeability in vacuum, I is the current passing through the solenoid and N_z is the number of axial turns the solenoid is made of, and l is the length of the solenoid. Assuming a constant distance between the solenoid and the permanent magnet the magnetic force F_m is proportional to the current, I, as in Equation (2.14), since J_2 is proportional to the electric current [10].

$$F_m \propto I \tag{2.14}$$

2.5.3 Distance Parameter

The force acting between a permanent magnet and a solenoid also depends on the distance between them. Figure 2.6 illustrates the distance d, where d is measured from the

bottom of the permanent magnet to the top of the solenoid. In this case the distance can be negative since the diameter of the permanent magnet is smaller than the inner diameter of the solenoid and can therefore be lowered into the solenoid, to a "negative distance". The force distribution for a variable distance d is seen in Figure 2.7 by the thick line, which indicates that the largest force acting between the objects are at $d = 0m$ [11].

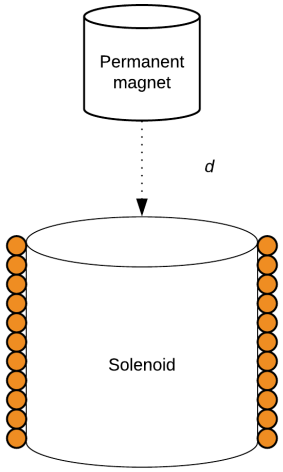

FIGURE 2.6: Illustration of the distance between a permanent magnet and a solenoid. The permanent magnet fits within the solenoid which allows the distance d to be negative.

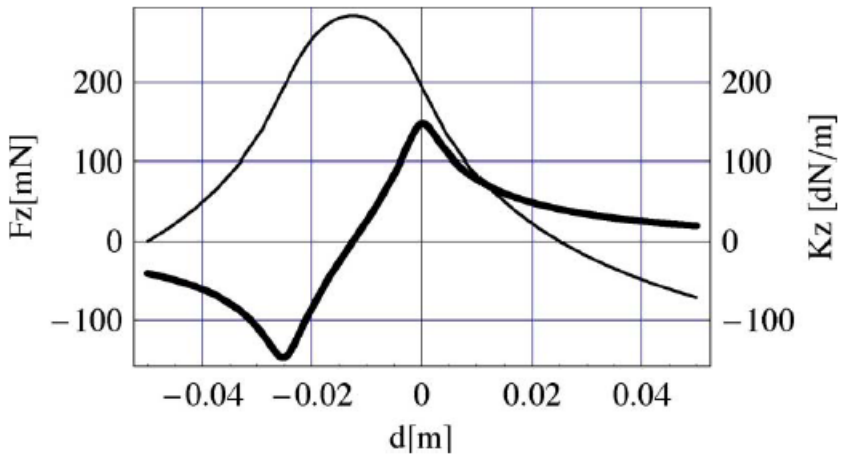

FIGURE 2.7: The thick line illustrates the force distribution along the distance d. The maximum force acting between two magnets are at distance $d = 0m$. *R.Ravaud et al. "Cylindrical Magnets and Coils: Fields, Forces and Inductances"* [11].

2.5.4 Solenoid Design Parameters

Design parameters that affect the magnetic force are the number of turns, length and diameter of the solenoid. All three parameters are dependent of each other, since e.g. more turns increases the diameter. It is also necessary to consider that a solenoid with fewer turns, and therefore also less length of wire, has a lower resistance. A lower resistance leads to higher current considering Ohm's Law ($I = \frac{U}{R}$), this could seem to lead to an increase in the magnetic field magnitude of the solenoid. Considering that the magnetic field magnitude is also proportional to the number of turns [12], it is realised that there is a trade-off between the dimensions of the solenoid and the current magnitude.

2.6 Discussion of Other Solutions

Since the new principle for the flow sensor is based on the function of a rotameter, several articles on flow measurement with a rotameter as its basis have been studied. The general idea in most of them is to measure the displacement of the float in different ways and transmit an electrical signal [2], [3] and [13]. No articles were found where the idea was to keep the float in a fixed position.

The new principle of the flow sensor has some elements of magnetic levitation which prompted a search for articles on the subject [14]. This was however not prioritized since optimal position control of the float is not vital. Focus was instead shifted to better understanding the equations for the flow which would be primary task to control. Thus an article on flow in a rotameter [4] was studied to get an idea of what to start testing first.

3 Sensor Design

This chapter describes the design of the new flow sensor's different hardware components, concept generation of designs, and simple tests. The sections refer both to previously presented theory as well as the results of appended tests. The idea of the new flow sensor, as described earlier, is to use magnetic force to create an equilibrium along with gravity, buoyancy force and drag force from the flowing fluid. The magnetic and drag force components each require some essential parts in the design. The possible magnitudes of these also set a few boundaries for how the different components can be designed.

3.1 Sensor Components

From the initial idea of solution for flow measurement there are some components that are identified as prerequisites for the flow sensor to function. The components are:

- *Float* - is affected by all four forces. Mainly designed considering the drag force. The float needs to be magnetic or ferromagnetic.
- *Solenoid* - affects the float with a magnetic force.
- *Position sensor* - determines the position of the float.
- *Frame* - acts as the tube for the float to be positioned in, holds the solenoid in place and holds the position sensors in place.
- *Solenoid driver* - controls the current to the solenoid.
- *Electric current sensor* - measures the current applied to the solenoid.

3.1.1 Float

While designing the float, there are a some parameters to consider. Different shapes create different drag forces. Furthermore, the behaviour of the float when placed in a tube with flowing fluid needs to be analysed. For a vertically placed tube, the float should remain as vertical as possible and not wobble too much. Apart from the shape, the size of the gap between the float and the tube affects the flow needed to lift the float. With different dimensions of the float, the tube and float together represents different hydraulic diameters. The smaller the hydraulic diameter is in relation to the diameter of the tube, the higher the fluid velocity is. Thereby the drag force affecting the float is also larger.

The second issue to address is the magnetism. To achieve a magnetic float a permanent magnets is placed inside. The magnitude of the force that can be achieved between the permanent magnet and the solenoid depends on the magnetic fields from both the solenoid and the permanent magnet. Given a certain distance between the solenoid and the permanent magnet, the same attracting force can be achieved by either using two magnets with equally strong magnetic fields or by having either of them to be stronger and the other weaker. The magnetic fields of the two must achieve a force between them that is within the desired region. The decision on material and size of the magnet in the float must thus be made together with the design of the solenoid and the float.

The magnetic and the drag forces need to be balanced to get a good result. A weak magnetic force, may not be able to keep hold of the float against the fluid flow. The drag force needs to be at least of the magnitude needed to lift the float at the lower bound of the target range of the sensor. It should not be too strong, as a strong drag force corresponds to a large pressure drop which is not desirable.

The buoyancy and the gravity are more or less constant forces on the float. These two forces together create a resulting force that either acts against the drag force or against the magnetic force, depending of the material and design of the float.

3.1.2 Solenoid

Equation (2.13) in Section 2.5.2 states that the design parameters for a solenoid is the number of turns and its length. The design and dimension of the float and the tube sets a boundary for the inner diameter of the solenoid. Equation (2.13) also states that the magnetic field is determined by the electric current applied, which the new principle is based on. The amount of current applied for a given voltage is determined by Ohm's law. The resistance of the solenoid is determined by the length of the copper wire and its thickness.

The size of the new sensor is supposed to be small, which sets some undefined dimensions for the solenoid. This means that the solenoid has to have a reasonable size to be fitted inside an HD machine.

3.1.3 Position Sensor

The new principle is based on keeping the float in a fixed position. A function to measure the position of the float is necessary. The position sensors needs to be placed on the frame, outside of the tube. Advice from employees at Baxter is that optical distance measurement is tricky in this case since it gets disturbed due to fouling.

3.1.4 Frame

A frame is needed to form the tube for the float, hold the solenoid in place and allow attachment of position sensors. The design of the frame depends on the dimensions of the float, the solenoid and which position sensors are used. For a given design of the float, there is a specific range of inner diameter of the frame which achieves good conditions for the flow. As for the exterior of the frame, the ability to hold the solenoid together and

ability to mount sensors and other parts on it are important factors. In early testing some additional features found to be practical are a support at the top of the sensor which let the fluid flow through, even if the float reaches the top of the tube. Also, to easily observe the behaviour of the float a transparent frame is practical.

3.1.5 Solenoid Driver

To control the magnetic field from the solenoid, the current to the solenoid needs to be controlled. If the sensor is to be controlled by a generic micro controller, outputs can only source low current which is not sufficient to drive the solenoid. Therefore, a circuit to amplify the signal to the solenoid is needed similar to a motor driver. The amplifier can either operate by a linear analogue signal or PWM signal.

3.1.6 Current Sensor

The new principle needs to measure the current given to the solenoid. A generic micro controller can not measure electric current, but it can measure analogue voltage. Therefore, the current needs to be measured with a circuit that transmits a corresponding voltage signal.

3.2 First Prototype and Tests

The first prototype of the flow sensor had been made before the project started by the supervisor. The first prototype gave an idea of the concept, its desired dimensions and design.

3.2.1 Design

The first prototype of the frame is lathed from a plastic rod. In the middle of the rod a hole through the entire length is drilled, to create the tube which the float is placed in. At the outside of the frame there are some guides to hold the solenoid in place. The frame also has two connection caps to allow silicone tubes to be connected.

The float is constructed of a plastic rod which is lathed to a cone. Inside the cone a drilled hole makes room for a neodymium permanent magnet. The magnet is secured with a lid that covers the hole.

3.2.2 Tests

The float is cone shaped, similar to the ones in an ordinary rotameter. The supervisor had done some tests with the initial float design. In those tests, the float had gotten jammed inside the tube of the flow sensor. Either because of being dragged to the top end of the tube, or by turning in the tube and jam itself stuck in the middle of the tube. The gap between the float and the tube is tight in this prototype.

With this first prototype the ability to hold a float in place was tested. The prototype managed to hold the float in place. When current is applied through the solenoid it

becomes warm, due to heat from power loss in the copper wire. At a current over $0.4A$ the solenoid becomes too warm, which might cause damage to the sensor construction.

3.2.3 Conclusion

The first prototype confirmed that the solenoid can hold the float in place. The prototype also showed a desired size of the sensor. Tests indicated that the gap between the float and the tube is too tight, and that a cone shaped float might be problematic if it turns and gets stuck. Another problem with the first prototype is that it is not transparent, which makes it difficult to determine the behaviour of the float inside the tube.

3.3 Float Design

From the theory of flow in a rotameter [4] a lot of references were made to the importance of validating the theory with empirical studies. Finding a good shape for the float is thereby decided to be the result of various tests. Two hypotheses extracted from theory are considered in concept generation and testing.

3.3.1 Hypothesis of Float Shape

Consider Equation (2.4), Reynolds number change due to velocity of the fluid, which affects C_D as well. By examining Figure 2.4 it is seen that C_D is constant for a disk already at a Reynolds number of 600, while a streamlined body gets a constant C_D at 200 000. From this and previous theory two hypotheses are made:

1. A disk shaped float e.g. a cylinder has a constant C_D, hence the drag force follows a relation for the fluid velocity in square.

2. A streamlined float has a smaller contribution from $C_{D,pressure}$, due to smaller wake transformation. Therefore, the drag force might be more predictable.

3.3.2 Float Concept Generation

Different kinds of geometrical shapes, mostly rotationally symmetrical, are designed and produced with the help of an in-house workshop technician. The different designs are presented in figures 3.1 to 3.6 below. In the figures, the direction flow is assumed to be from left to right. All floats are manufactured to hold a permanent magnet inside its body. The floats are lathed from a rod made of polyether ether ketone (PEEK). The magnets placed inside are neodymium (NdFeB) magnets. To give the float a low centre of gravity the magnets are placed as low in the float as possible. Since the magnets have a higher density than the plastic, this should lower the centre of gravity.

FIGURE 3.1: Cylindrical float.

FIGURE 3.2: Cone float.

FIGURE 3.3: Cone float with cylindrical extension.

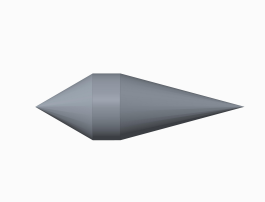

FIGURE 3.4: Double sided cone float.

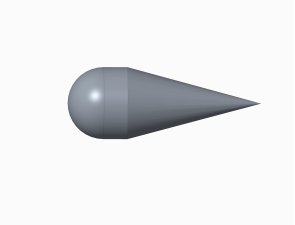

FIGURE 3.5: Streamlined float with spherical front.

FIGURE 3.6: Cone float with rear guides.

The cone float seen in Figure 3.2 is the initial float design supplied by the assistant supervisor. The other designs are created with a few different goals. Different shapes of the front and rear has different impact on the drag force through C_D([5] (p.498). The different concepts are designed to create different combinations of front and rear shapes. The designs are explained in the following list:

- **Cylindrical Float** - The straight cylindrical float, Figure 3.1, is designed to be very blunt and non streamlined. This shape tests the hypothesis that a disk has a constant drag coefficient at low Reynolds numbers. With a constant drag coefficient the drag force should be proportional to the fluid velocity in square, Equation (2.7). The cylinder is also the most simple rotationally symmetrical shape.

- **Cone Float** - The cone float 3.2 is the same design as used in the first prototype. This design is common in ordinary rotameters. Since it is common in rotameters it is assumed to be thoroughly investigated.
- **Long Cone Float** - The goal of the long cone float, Figure 3.3, is to have the same stability of the cylinder, but also the sharp, cutting front of the cone float. The long body makes the float more rigid than the shorter cone float.
- **Double Sided Cone Float** - The idea of the double sided cone float, Figure 3.4, is to obtain a more streamlined design compared to the cylinder and the long cone. There is also the idea to keep the shapes simple and easy to manufacture. This is designed to test hypothesis 2.
- **Spherical Front Float** - As a further development of the double sided cone the float in Figure 3.5 with a hemisphere replacing the front cone is designed to potentially decrease the drag of the float even more. This is designed to test hypothesis 2 as well.
- **Cone Float with Rear Guides** - The cone float with rear guides, Figure 3.6, is a design made to improve the stability of the cone float. The idea is to prevent turning inside the tube and jamming at a crooked angle. Due to the complexity of manufacturing the float, it is initially left at the concept stage.

3.3.3 Float Testing

To see the behaviour of the prototype floats, when inside a tube with flowing liquid, the floats are put in a semi clear tube connected to a water tap. The tube used is wider than the tube of the first prototype. Therefore it is not certain that the tests gives any hard, useful results. However, it is a way to get an idea on the behaviour of the floats in flowing liquid. The procedure for the tests is to create a flow through the tube, which is held vertically. When an estimated adequately high flow rate is achieved, one of the floats is placed in the tube. The flow rate is modified until the float is kept at a constant height, or very close to constant. While keeping the float at constant height, the behaviour of the float is observed. The observations are:

- **Cylindrical Float** - Very stable. Low flow needed to keep constant height.
- **Cone Float** - Fairly stable though at times wobbly. High flow needed to keep constant height.
- **Long cone Float** - Very stable. High flow rate needed to keep constant height.
- **Double Sided Cone Float** - Quite wobbly. Low flow rate needed to keep constant height.
- **Spherical Front Float** - Less wobbly than the double sided cone float, but not stable. Low flow rate to keep constant height.

The test results are based on observations, and measuring the flow rate by measuring the time to fill a beaker with 1 litre. High and low flow rate is based on the comparison between the tests. From these quite uncertain tests, the main result to take note of is the stability of the floats. The features that seem to correlate with a stable position of the float is its length and the shape of the top end. The longer the float, the better stability is achieved and there is also seemingly better stability of floats with flat tops. Streamlined floats are more unstable in these tests.

3.3.4 Float Choice

The desired behaviour of the floats is to be stable and to not wobble in the tube. Since the diameter of the tube is not the same that is to be used in the sensor, the flow rate which is required to keep a constant height is not vital to consider. The float designs with best behaviour are the *cylindrical float* Figure 3.1 and the *long cone float* Figure 3.3, since they are very stable. It is decided that these two shapes is used to test the new principle. The second hypothesis in Section 3.3.1 is decided to not be further tested at this point, since the streamlined floats seems to be unstable.

3.4 Solenoid Design

The goal for the design of the solenoid is to determine its dimensions. If the solenoid becomes to weak it can not hold back the float against the fluid flow. The operating position for the float is also considered when determining the dimensions. The length, inner diameter, outer diameter, number of turns of the solenoid are dimensions that need to be determined. For a solenoid the packing density together with wire thickness affect the outer diameter for a specified number of turns, inner diameter and length.

3.4.1 Solenoid Concept Generation

Three different dimensions of the solenoid are generated. The dimensions of the solenoids are given in Table 3.1. The dimensions changed between the designs are the length and the number of turns. These changes affect the length of the wire, which affects the resistance in the solenoid. The inner diameter for the solenoids are set to $11mm$, since tests with first prototype showed that this dimension is suitable. The maximum outer diameter is set to $25mm$, since this is the diameter of the transparent rod from which the frame is made and is therefore the maximum diameter of the solenoid guides.

The number of turns is matched to obtain an outer diameter of $25mm$ for a specific length. The number of turns needed for the solenoid is calculated with "Production Solution" free on-line calculator [15]. The packing density is assumed to be as good as possible.

The three different concepts generated can be seen in Table 3.1. The main difference between these concepts is the length. Since the inner and outer diameter is the same, the number of turns changes with a varying length. The wire thickness is chosen to $0.25mm$, since the first prototype uses this dimension.

TABLE 3.1: Different designs of solenoid for simulation

	Length [mm]	Number of turns	Resistance [Ω]
Design 1	31.5	2900	64
Design 2	20	2250	44.69
Design 3	30	3350	66.54

3.4.2 Solenoid Simulation

Analyses of the properties of different solenoid designs and magnetic floats are needed. As magnetic field theory is complex, simulations are often made, *FEMM 4.2* is used to simulate the magnetic field of the solenoid and the magnetic float. The magnetic flux density affects the force acting on the permanent magnet. The different designs of the solenoid are simulated with a fixed current of $0.1A$ and a wire thickness of $0.25mm$. The set-up for the simulations is seen in Figure 3.7. The simulation is axisymmetric.

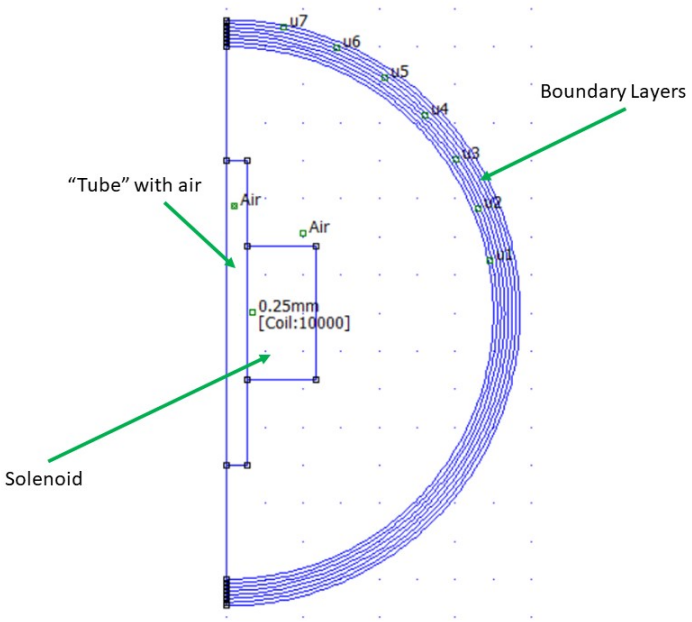

FIGURE 3.7: Simulation set-up.

Results of Solenoid Simulation

Figures 3.8, 3.9 and 3.10 show the simulation results. Higher magnetic flux density results in a larger force acting on the permanent magnet placed in the tube. At a distance $40mm$ in Figures 3.8, 3.9 and 3.10 the magnetic flux density is equal to zero. If the permanent magnet is placed at this distance no force acts on it.

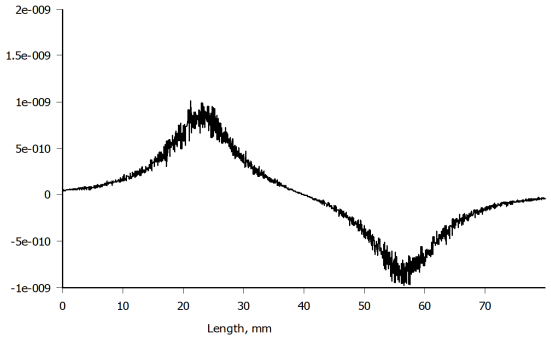

FIGURE 3.8: Design 1. Magnetic flux density.

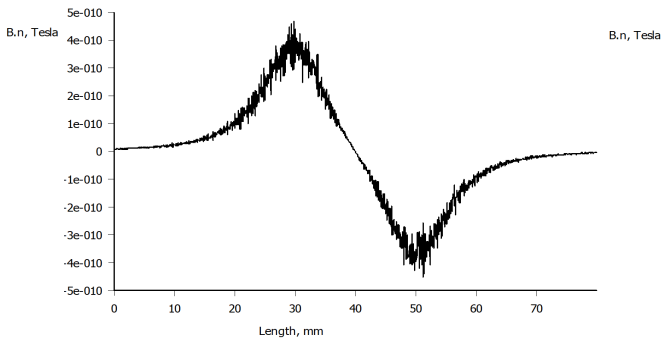

FIGURE 3.9: Design 2. Magnetic flux density.

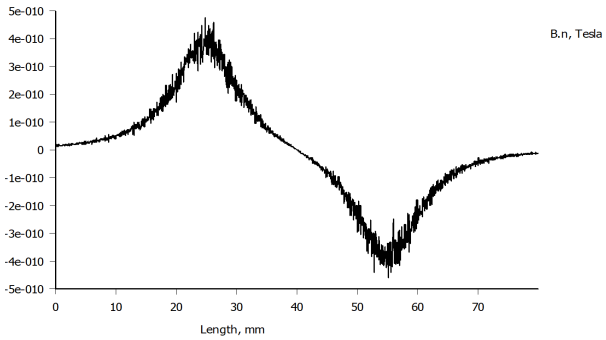

FIGURE 3.10: Design 3. Magnetic flux density.

Section 2.5.3 shows that the maximum radial magnetic flux density occurs at the end points of a solenoid. Since the magnetic flux density is proportional to the axial force acting on the float, the float is affected with maximum force at the end points of the solenoid. Results from the simulations also shows that the maximum magnetic flux density occurs at the end points of the solenoid.

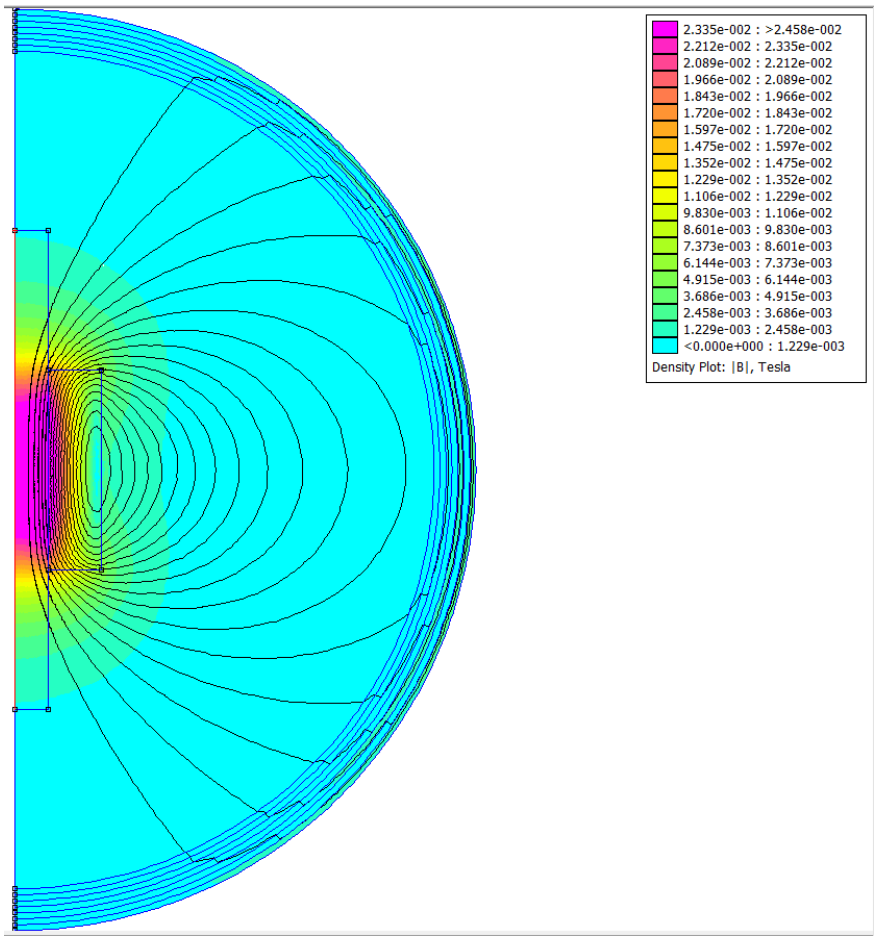

FIGURE 3.11: Simulation of second prototype magnetic flux distribution in solenoid.

Figure 3.11 illustrates how the magnetic field is distributed in the the solenoid and surrounding air. In Figure 3.12 the same solenoid is simulated but with a permanent magnet placed in the tube. It is seen that the permanent magnet contributes with a stronger magnetic field than the solenoid.

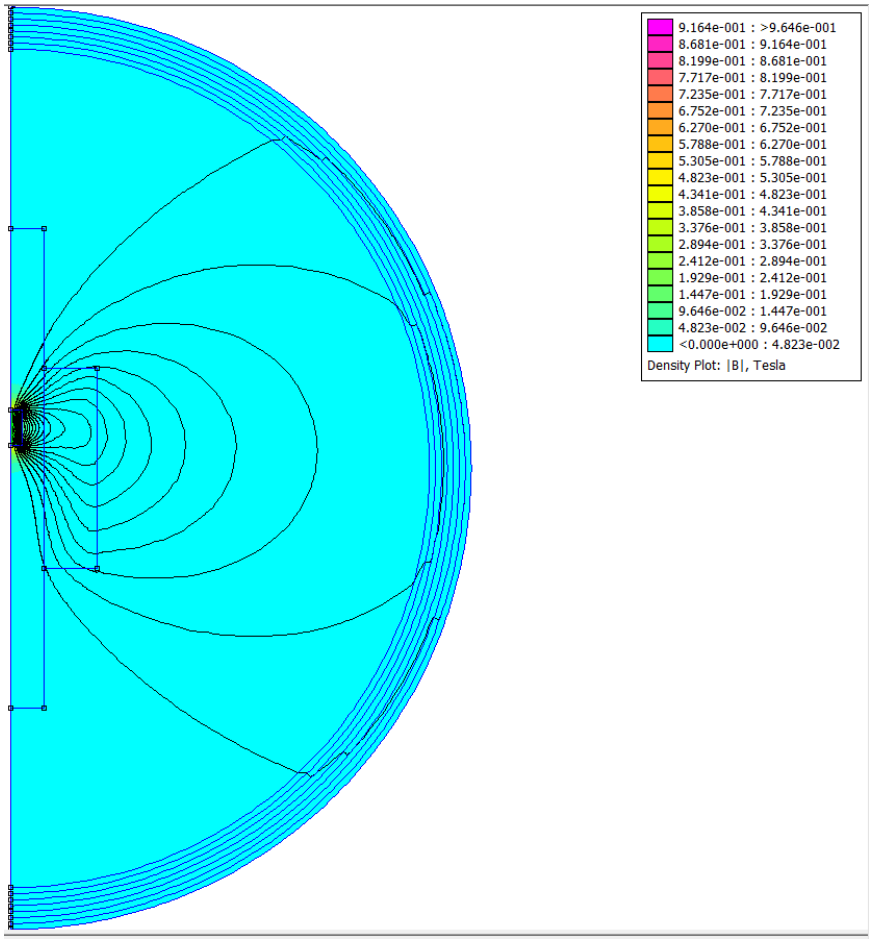

FIGURE 3.12: Simulation of second prototype magnetic flux distribution in solenoid with a permanent magnet.

To achieve a magnetic float either a permanent magnet or an iron core can be placed inside it. In Table 3.2 simulation of the force acting on the float is simulated with both a permanent magnet and an iron core with the same solenoid. The force is much larger with the permanent magnet, hence the solenoid can be weaker to achieve the same magnitude of the force.

TABLE 3.2: Simulation of force acting on a permanent magnet and a iron core placed inside a solenoid.

	Force [mN]
Permanent Magnet	9.3
Iron Core	0.4

3.4.3 Solenoid Choice

When choosing the final design of the solenoid, the operation position of the permanent magnet needs to be considered. Figure 3.13 shows where the *desired position* and the *operating section* in the magnetic flux density is located. At this position a downward force acts on the permanent magnet. If the permanent magnet moves a bit to the top of the tube (meaning that the distance decreases in Figure 3.13) a larger force acts on the permanent magnet without increase of electric current in the solenoid. It is preferable for the control of the floats position that the magnetic flux density in the operating section is linear, or almost linear. Then the force acting on the permanent magnet is linearly proportional to the floats position in the solenoid.

TABLE 3.3: Dimensions for the chosen solenoid design.

	Final Design
Inner Diameter	11 mm
Outer Diameter	25 mm
Length	31 mm
Number of Turns (Approximately)	2650
Resistance	54 Ω

Studying Figure 3.8, 3.9 and 3.10 it is seen that *Design 2* has a smaller operation section, but is more linear than *Design 1* and *Design 3*. *Design 1* and *Design 3* has a larger operation section but less linear distribution of magnetic flux density. *Design 3* is chosen since its distribution is more linear than *Design 1* and the operation section is larger than *Design 2*. The final dimensions of the manufactured solenoid is seen in Table 3.3.

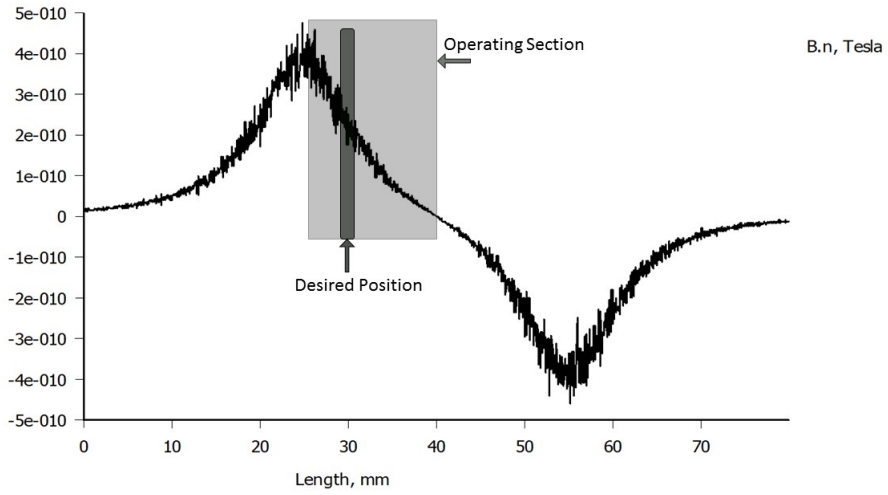

FIGURE 3.13: Operating section is the section where the permanent magnet can operate. Desired position is where the operation position should be set.

3.5 Position Sensor

The new flow sensor is intended to measure the fluid flow rate in a hemodialysis process. In this process the liquid contains electrolytes and other substances. Theses substances can create fouling in the system. As mentioned before, position sensors operating by optics are not suggested, since employees at Baxter previously have experienced problems with obstructions of the view for these sensors. Since a permanent magnet is placed inside the float, Hall effect sensors are practical, and proposed by Baxter employees to use since they can be placed outside of the flow path and are not sensitive to layers obstructing the view.

The Hall effect sensors detects magnetic fields and transmit an analogue signal. The analogue signal changes by the magnitude of the magnetic field. A permanent magnet with constant strength affects the Hall effect sensor with different magnitude depending on its distance from the sensor. The Hall effect sensor can then be used to determine the distance to the permanent magnet even in fluids that are prone to fouling. The Hall effect sensor is therefore used to measure the floats position.

3.5.1 Position Test

The Hall effect sensor is a *55100-AP-02-A Miniature Flange Mounting Proximity Sensor* from *Littelfuse*. With cable ties and double-sided tape the Hall effect sensors can easily be attached to the prototype. The sensor is supplied with 5V and transmits an analogue signal between 0V to 5V depending on the proximity of the permanent magnet and what direction its poles are facing.

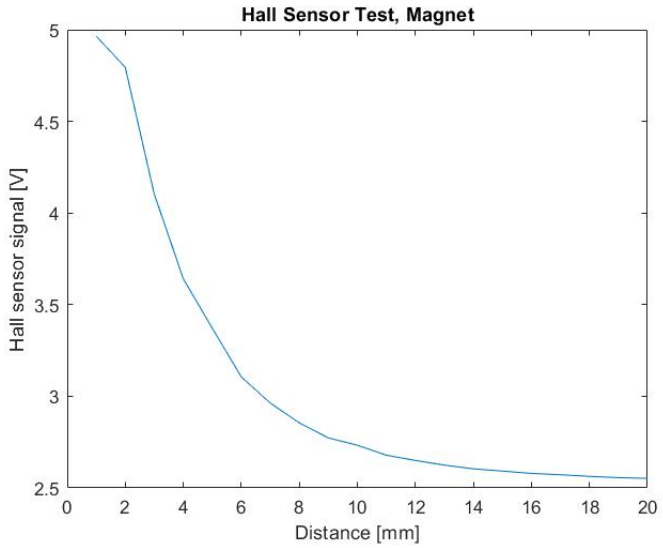

FIGURE 3.14: Transmitted signal from a Hall effect sensor for different distances to a permanent magnet.

The Hall effect sensor is tested to see how it transmits the analogue signal depending on the distance to the permanent magnet, the result is seen in Figure 3.14. In Figure 3.14 it is seen that the Hall effect sensor can detect the magnet, but at a distance around 20 mm the Hall effect sensors do not detect the magnet any more. The Hall effect sensor transmits a signal of 2.5 V when no magnet is present.

The new sensor needs to measure the position of the float either continuously or at frequent intervals. It is necessary to determine if the Hall effect sensors can position the float while current is applied to the solenoid, or if the current needs to be switched off for a short period while the position is measured. Comparing Figure 3.11 and 3.12 it is seen that the permanent magnetic field is significantly stronger than the field from the solenoid. If the permanent magnetic field is stronger it indicates that it is possible to determine the permanent magnets position in the tube when current is applied to the solenoid. In Figure 3.15 tests conducted to determine the position of a permanent magnet while current is applied to the solenoid is presented.

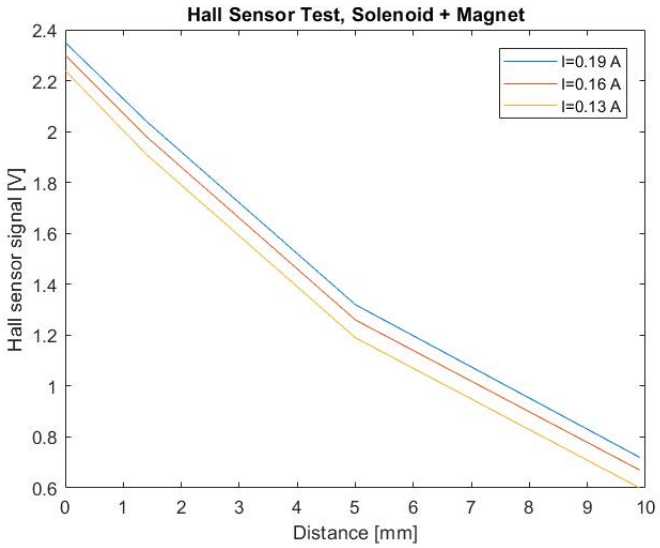

FIGURE 3.15: Transmitted signal from a Hall effect sensor for different distances to a permanent magnet, when different currents is applied to the solenoid.

Figure 3.15 indicates that the Hall effect sensor can detect the position of the permanent magnet while current is applied to the solenoid. Different magnitude of current offsets the measurement, but not too much to not be able to sense the permanent magnet. Test results presented in Figure 3.16 show that the Hall effect sensor reading is linear to the current applied to the solenoid. The offset in Figure 3.15 is then just a linear offset proportional to the current applied. Full description and data from the tests are attached in Appendix B.

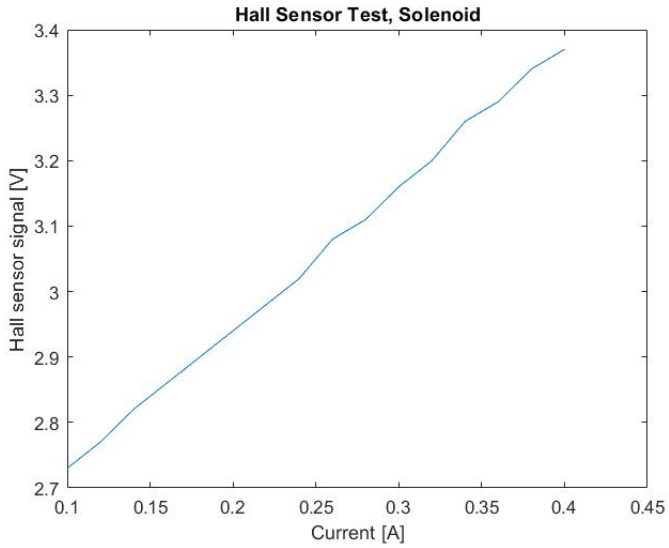

FIGURE 3.16: Plot of Hall effect sensor measurement signal versus current in the solenoid.

To be able to handle interference of surrounding magnetic fields, two Hall effect sensors can be used. The interference offsets the two sensors equally and the difference between the two can then be used regardless of offsets from the interference.

3.5.2 Position Sensor Conclusion

The conclusion from tests with the Hall effect sensor is that it is possible to position the float while current is applied to the solenoid. Two sensors should be used to handle interferences. The offset caused by the magnetic field from the solenoid needs to be compensated for in the software.

3.6 Frame

The frame creates the tube for the float, guides for the solenoid and attachments for position sensors. The gap between the float and the tube needs to be tight enough for the float to rise at a specific flow rate. If the gap is too tight the solenoid might not be able to keep the float in fixed position.

The first prototype is presented in Section 3.2. The conclusion from tests conducted with the first prototype is that the behaviour of the float is easier to analyse if the frame is transparent, and that the gap between the float and the tube needs other dimensions. The transparency does not add any other features and is not necessary for the principle more than to simplify experiments.

3.6.1 Second Prototype

To test the new principle a simple prototype with correct dimension is built. The *Second Frame Prototype* has a plastic transparent tube, and cardboard to support the solenoid. This prototype is used as a proof of concept for the principle, before a more robust prototype is manufactured.

In Section 5.1.2 tests with this frame is conducted, to show the proof of concept. The tests results in a lift for the float around 500 ml/min, and not 300 ml/min as desired. The reason for lift around 500 ml/min is due to a gap between the float and the tube that is to large.

3.6.2 Third Prototype

Results from *Second Frame Prototype*, presented later in Section 5.1.2, indicate that the new principle works. The *Third Frame Prototype* is designed with a tighter gap between the float and the tube than the *Second Frame Prototype*, to achieve lift before a flow rate of 300 ml/min.

Tests with the third prototype showed that its dimensions create a satisfyingly narrow gap and achieves the desired behaviour in lift and drag force on the float (Section 5.1.2). The third prototype of the frame combined with the solenoid design manages to lift and hold the float in the range of 300 ml/min to 800 ml/min. The third prototype is chosen as the final design, and is used to evaluate the new principle.

3.7 Solenoid Driver

To keep the float in a fixed position the magnetic field from the solenoid needs to be controlled. The magnetic field is controlled by changing the current given to the solenoid. As for motors the solenoid needs a driver which amplifies a control signal.

The position sensors are Hall effect sensor, which also senses the magnetic field from the solenoid. In Section 3.5.2 it is concluded that the Hall effect sensors can measure the position of the permanent magnet while current is applied to the solenoid. Since the position sensor operates well while the solenoid generates a magnetic field, the solenoid driver only needs to be a simple amplifier. If the position sensors would not sense the permanent magnet, the magnetic field from the solenoid needs to be switched off for a period when the sensor reading is conducted. To switch off the solenoid and burn its energy fast requires a more complex solenoid driver.

3.7.1 Solenoid Driver Choice

To drive the solenoid a *Centent CN0122* 4 quadrant motor drive is chosen. The *Centent CN0122* is a linear amplifier and does not operates using PWM. The *Centent CN0122* is set to torque control. The *Centent CN0122* is chosen since it is simple to connect to the solenoid and to the test rig. Other amplifiers are also possible to use.

3.8 Electric Current Sensor

The new principle needs to measure the current applied to the solenoid. The solenoid driver is isolated from the common ground, hence it is important to use a circuit that handles large common mode offsets. After consultancy with a senior electrical engineer at Baxter it was decided that an INA117 would be used to measure the current. INA117 handles large common mode offsets and transmits an analogue output linear to the current. The circuit for current measurement is seen in Figure 3.17.

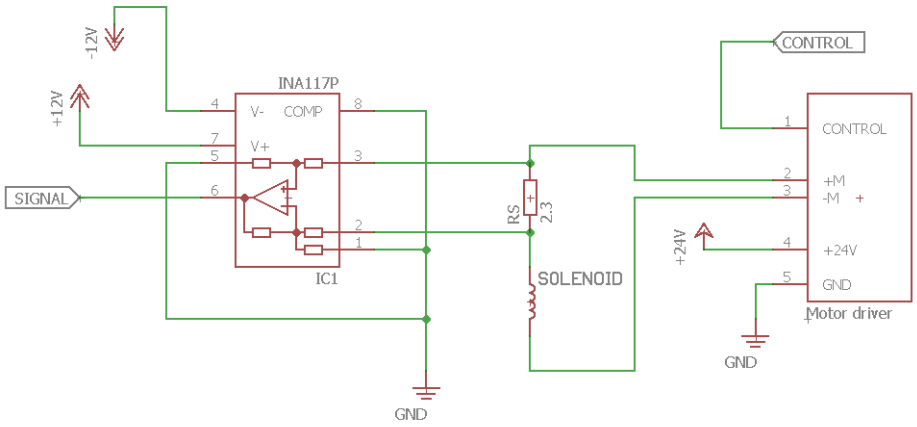

FIGURE 3.17: Circuit schematic for current sensor and solenoid driver.

The resistor R_S value is 2.3Ω. The corresponding transmitted analogue signal from INA117 is given by Equation (3.1).

$$U(I) = R_S I \tag{3.1}$$

Where U is an analogue signal proportional to the current I.

3.9 Final Design

In Figures 3.18 and 3.19 a rendered model of the final design can be seen. The final design has a transparent tube and the Hall effect sensors are attached with cable ties and double-sided tape. At the top and bottom of the tube some stops are inserted to allow the fluid to pass when the float is at these positions. Complete drawings of the frame and floats are in Appendix C.

FIGURE 3.18: Final design of the sensor

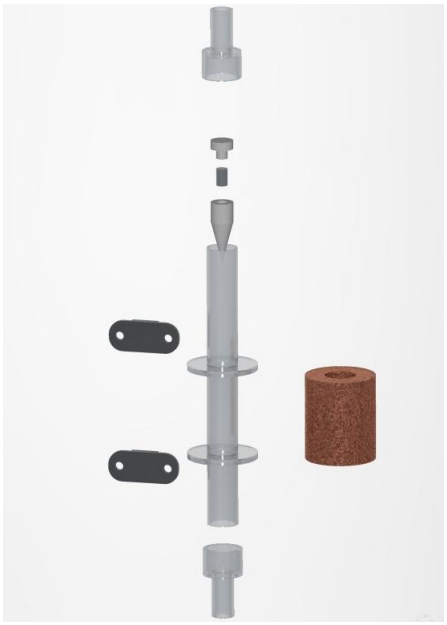

FIGURE 3.19: Final design of the sensor, exploded view.

3.10 Control Software

For the sensor to operate positioning and controlling of the float is needed. The new sensor also needs a model between the fluid flow rate and the electric current. The programming was made in Simulink.

3.10.1 Positioning

The new principle is based on keeping the float in a fixed position, hence the position of the float needs to be determined. The electric current applied to the solenoid is controlled based on the position measurement.

Hall Effect Sensor Scaling

The Hall effect sensors can measure the position of the float when current is applied to the solenoid. When current in the solenoid changes, the Hall effect sensors detects this and relates it to a new position for the float. The magnetic field from the solenoid needs to be ignored to determine the correct position of the float. The Hall effect sensor reading from the magnetic field of the solenoid is linearly proportional to the current applied.

The gain of the linear correlation is found by experiment. The gain of the measured current is subtracted from the reading of the Hall effect sensor. This way the magnetic field from the solenoid is ignored.

Magnetic Force Control

The new sensor is supposed to measure a constant fluid flow rate and does not need to be optimized to handle large steps. Therefore a PI controller is used to control the electric current. The PI controller is a discrete PI controller block from the Simulink Block Library 9.0. The parameters are tuned by visual study of the float until it behaves as desired.

3.10.2 Filtering

To have stable signals to work with, some filtering is required. The signals from the sensors used are more or less noisy. To filter out the noise a third order Butterworth filter, designed with Mathworks filterDesigner, is used. The filters have a sampling frequency of 1000 Hz as the rest of the Simulink model and a cut off frequency of 10 Hz. No analogue pre-sampling is used since no disturbances at frequencies above 500 Hz were found with significant amplitudes.

4 Test Rig

To test and validate the new principle a test rig is used. The test rig consists of several sensors and actuators to control and to monitor the system. The sensors and actuators are connected to each other by silicone tubes to create a flow path for the fluid. Signals from the sensors and actuators are connected to a HIL (Hardware-in-the-Loop) target machine, which controls and gathers data from the system. The test rig also consists of some necessary components to drive and supply power to the sensors and actuators.

4.1 Test Rig Frame

The frame for the test rig (already assembled by Baxter before the start of the project) consists of aluminium profiles. On the front, actuators and sensors are mounted. On the rear, separated with a plastic screen, DIN rails are placed for mounting electronics.

The flow path and the components of the front side are illustrated in figure 4.1. The numbers in the component list corresponds to the numbers in the figure. Components A, B and C are a separate system to control the temperature of the system. Electronics and components mounted on the rear of the test rig are:

- *HIL target machine*
- *24VDC AC-DC converter*
- *5VDC DC-DC converter*
- *±12VDC DC-DC converter*
- *Relay*
- *Motor driver*

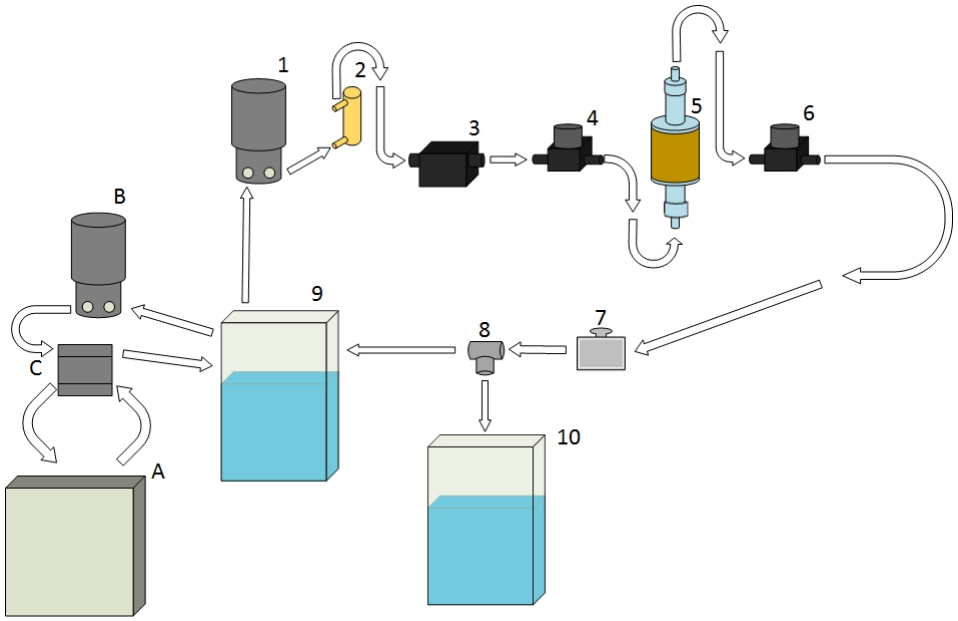

FIGURE 4.1: Flow chart describing the test rig. 1) Pump, 2) Rotameter, 3) Electromagnetic flow sensor, 4) Pressure sensor 1, 5) New flow sensor, 6) Pressure sensor 2, 7) Trim valve, 8) 3-way valve, 9) Water reservoir for circulation, 10) Water reservoir for scale measurement. A) Temperature controlled reservoir, B) Pump, C) Heat exchanger.

4.2 Flow Path

Figure 4.1 shows the flow chart of the system in the test rig. First, the *pump* draws water from a *reservoir*. The water is led through a conventional *rotameter* for a direct and visual feedback on the magnitude of the flow. Further along, an *electromagnetic flow sensor* is placed to give a digital and more precise measurement of the flow than the rotameter. Two *pressure sensors* are mounted on either side of the *new device*. After the second pressure sensor a *trim valve* is mounted to alter the pressure in the system. After the trim valve a *3-way electronic valve* is placed to make it possible to direct the water either back to the reservoir or to the *scale*. The scale is placed on a cart next to the rig, to avoid vibrations from the pumps.

4.2.1 Pump

The pump is a *Premotec* 24VDC motor connected to pump gears. The pump is controlled with a 4 quadrant motor driver. Two pumps are installed on the test rig, one to control the flow through the sensors, and the second to pump water through the heat exchanger.

4.2.2 Electromagnetic Flow Sensor

An electromagnetic flow meter from *Aichi Tokei*, is installed in the rig prior to the new flow sensor. The *electromagnetic flow sensor* is used as a reference during tests to see if the new flow sensor is drifting off from the supposed real flow rate.

The *electromagnetic flow sensor* uses an electromagnetic field to determine the speed of ions in the water. For an electromagnetic flow sensor to work, the liquid needs to be conductive. The *electromagnetic flow sensor* sensor uses open collector output to transmit a pulse, each pulse corresponds to 0.4611 ml. The flow rate can then be calculated by measuring the frequency.

4.2.3 Pressure Sensor

Two relative pressure sensors are placed in the system, one just before the new sensor and one right after. The pressure sensors are used to measure the pressure drop over the new sensor and to determine the pressure in the system relative to the atmosphere. The pressure sensors are from *Endress+Hauser*. The relative pressure sensors have a range between -0.933 to 1.6 Bar, and transmit an analogue signal between 0.71 to 3.94 VDC. The output signal is proportional to the pressure.

The pressure sensors are calibrated with a differential pressure sensor prior to testing. The calibration is implemented in software as a scaling factor and a bias in the linear model between the pressure and analogue output signal.

4.2.4 Valves

The *Trim valve* is a simple manual valve, which makes it possible to alter the operating pressure in the system since it is mounted at the near end of the flow path. The *3-way valve* is mounted at the very end of the flow path. This valve either directs the fluid back to the circulation reservoir or to the reservoir on the scale. The valve changes its outlet direction when 24 voltage is applied to it. The power supply is controlled via a *relay*, which is connected to the HIL target machine. The relay is controlled with a digital output signal.

4.2.5 Reservoirs

The two reservoirs for circulation and scale measurement are jerricans clad in bubble-wrap for insulation when conducting tests at temperatures far from room temperature.

4.2.6 Scale

The scale is used to weigh the amount of liquid that has passed through the system. The scale is a *Mettler Toledo ICS425*. The range of the scale is from 0 to 35 kg at a tolerance of 1 g. Between 0 to 7 kg the scale measures with a tolerance of 0.1 g.

The scale is connected to the target machine using RS-232 communication. The scale continuously transmits the current weight on the scale, with a sample frequency around 2 Hz.

4.2.7 Temperature Controlled Reservoir

A *Julabo F25-ME* refrigerated/heating circulator is installed to control the temperature of the water to the heat exchanger. The *Julabo F25-ME* has a range between -28°C to 200°C.

4.2.8 Heat Exchanger

A heat exchanger is used to control the temperature in the system. It is, on one side, connected to the test rigs second pump which pumps the water from the reservoir to the heat exchanger and then back to the reservoir. On the other side, it is connected to the temperature controlled reservoir. In the heat exchanger heat from a temperature controlled loop is transferred to the fluid in the test loop. The heat exchanger makes the system less dependent on the ambient room temperature, which might change over time. The heat exchanger also makes it possible to test the system at different temperatures. With a high flow rate in the temperature loop (higher than the flow in the test loop), the temperature of the fluid in the test loop can be controlled to be close to the temperature in the temperature controlled loop.

The temperature controlled reservoir could have been used as the circulation reservoir but for the fact that the volume of the heat controlled reservoir is not very large. Test performed by directing water to the scale would then be limited by that volume.

4.3 Electronics

The circuitry at the rear of the test rig consists of analogue and digital I/O signals. The talking points are the HIL target machine and the motor driver used to drive the pump. The other components as the power supply and the converters are standard components.

- **HIL Target Machine** - The *Speedgoat Baseline real-time target machine* is used for Hardware-in-the-Loop testing. The target machine creates a quick and easy way to run programs that are created in Simulink on hardware. Speedgoat Baseline has a 2 GHz quad core CPU and a FPGA. An I/O module connected to the Speedgoat Baseline provides a simple method to connect with hardware. The I/O module used in the test rig is IO397-50k. This I/O module supports analogue in and out, digital in and out, PWM out and PWM capture. The I/O module has 4 analogue in signals [16].
- **Motor Driver** To drive and control the pump a *Centent CN0122* 4 quadrant motor drive is used. The driver makes it possible to control the motor with an analogue signal from the target machine. The motor driver is set to speed control, such that the control signal controls the speed of the motor. Other settings available for *Centent CN0122* controller is torque control. The *Centent CN0112* is a linear amplifier which reduce its electrical interference, this makes it suitable for noise sensitive applications.

5 Sensor Evaluation

This chapter presents tests, results and analyses about the new principle. The tests are performed to investigate the initial questions determined in the scope. Also, it is investigated whether the system has any dependency on the parameters selected in the scope. The parameters are presented in individual sections. For each section and parameter, both results and analysis are presented. Before presenting the test results, the procedure for each test is explained.

The new sensor is equipped with two Hall effect sensors, but only the top sensor is used during the tests. The I/O module only has four analogue in ports, two are used for the pressure sensors, one for the electric current measurement and finally the last for the top Hall effect sensor. Tests with both Hall effect sensor show that this works as well, and using multiple sensors is believed to make the design less sensitive to interfering magnetic fields.

During the performed tests, a temperature of 23°C was the temperature control reference. A constant temperature is proven vital for good measurement and the ambient temperature made the uncontrolled system drift toward 23°C during the day. The temperature is chosen to differ only a little from the ambient temperature for better control and to be close to the "final" temperature of the day, as heating was easier than cooling. If nothing else is stated, the tests are run at a temperature of 23°C.

The conductivity is measured before the tests, concentrate or water is added to keep the levels around the same value. For all tests the conductivity was held around 16.7 mS/cm.

5.1 Proof of Concept

The proof of concept tests are conducted early, with the simple second prototype. They are conducted to determine if any relation between current and flow exists, and whether it is a linear, quadratic or another kind of relation.

5.1.1 Test Procedure

Before the test is initiated, the float is at rest at the bottom of the sensor tube. A small current is then applied to the solenoid so that it can catch the float as it moves upward. The fluid flow is then increased until it can lift the float i.e. until the drag force overcomes the resulting force between gravity and buoyancy. As the float rises, it soon reaches the solenoid and is held at equilibrium. At that point the solenoid controller is switched on, so that it maintains the desired position of the float. During the test, the solenoid keeps the float in place and the current through it is being measured, the fluid flow is measured by the electromagnetic flow sensor. The system is then ready for the actual testing. The fluid flow is gradually increased, manually, by increasing the control signal to the pump. After each increment in control signal, the system is allowed to set at a levelled out flow. This way, the majority of measurement data is collected at steady state positions. The flow is increased in this manner until the electromagnetic flow sensor measures the higher limit of the flow, 800 ml/min.

The first tests of the complete system are conducted with the second prototype of the frame and solenoid along with floats created to match the frames inner radius. The test is conducted for both the cylinder shaped float and the long cone float. Between the tests, the control parameters of the solenoid controller are tuned until the float shows a satisfactory behaviour. The raw data collected is too extensive to present, plots of current versus flow are presented instead.

5.1.2 Results

Figure 5.1 and 5.2 shows the plots of current measurement versus measured fluid flow. Figure 5.1 shows the test conducted with the the cylinder float, and Figure 5.2 shows the results when using the long cone float.

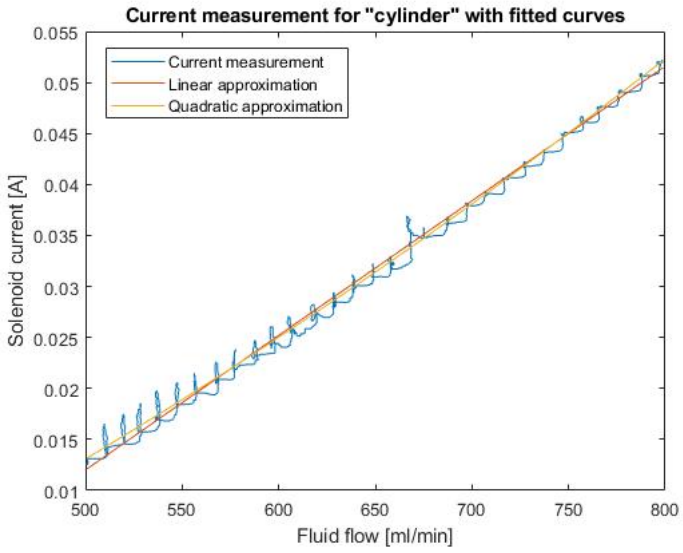

FIGURE 5.1: Fitted linear (red) and quadratic (yellow) curves along the current measurement for the cylinder float.

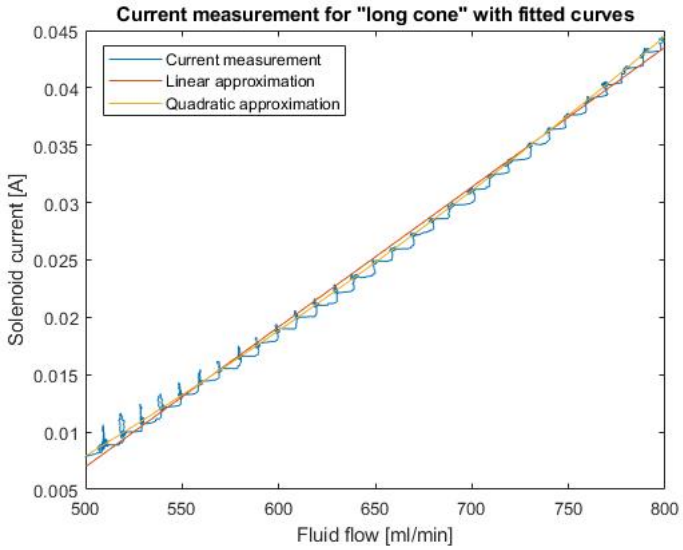

FIGURE 5.2: Fitted linear and quadratic curves along the current measurement for the long cone float.

The measurement data from Figures 5.1 and 5.2, is approximated with a linear and a quadratic model. The models are plotted, with respectively red and yellow lines, along with the measurements. The presented tests, conducted with the second prototype, are made in the range from 500 ml/min to 800 ml/min since the fluid flow can lift the float only above 500 ml/min approximately. The overshoot of the current curve are caused

by position control after flow changes. The following tests are performed with the third iteration of the prototype.

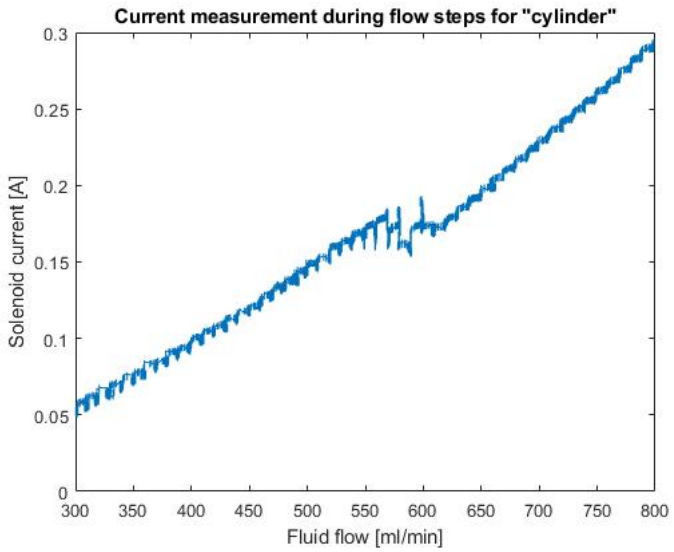

FIGURE 5.3: A graph of the current through the solenoid versus the fluid flow through the sensor. Measurement from tests using the cylinder float design in the third prototype frame.

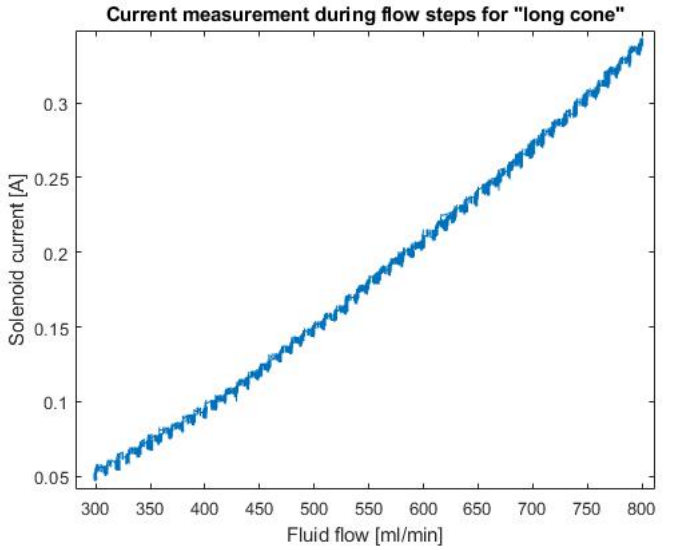

FIGURE 5.4: A graph of the current through the solenoid versus the fluid flow through the sensor. Measurement from tests using the long cone float design in the third prototype frame. The phenomenon occurring at 600 ml/min is discussed in Section 5.3.3

Test results from using the third prototype are shown in Figure 5.3 and 5.4. The third prototype manages to hold the float in the range from 300 ml/min to 800 ml/min. Figure 5.3 shows the results of using the cylinder float, and Figure 5.4 the results when using the long cone float.

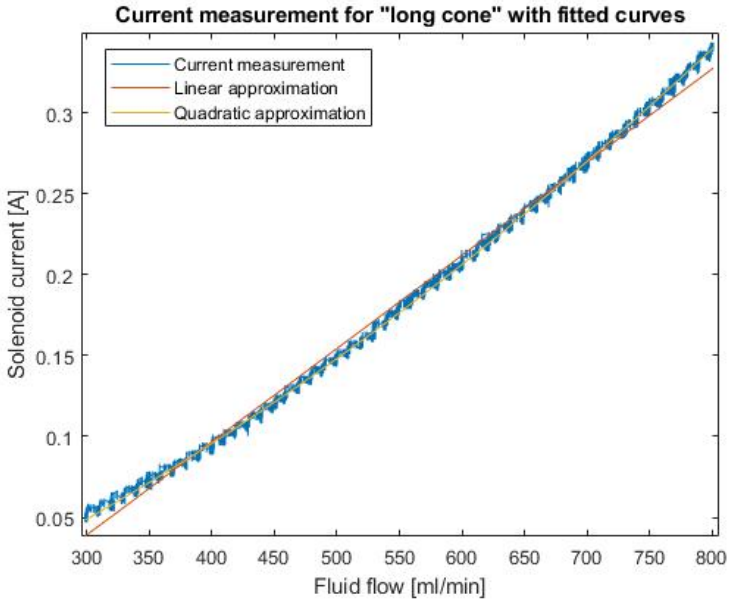

FIGURE 5.5: Fitted linear (red) and quadratic (yellow) curves along the current measurement for the long cone float design in the third prototype.

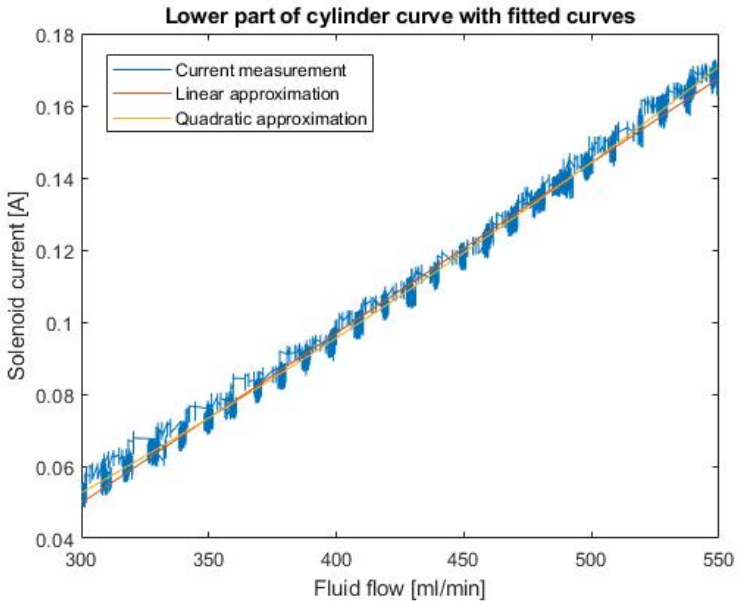

FIGURE 5.6: Fitted linear (red) and quadratic (yellow) curves along the lower part of current measurement for the cylinder float design in the third prototype.

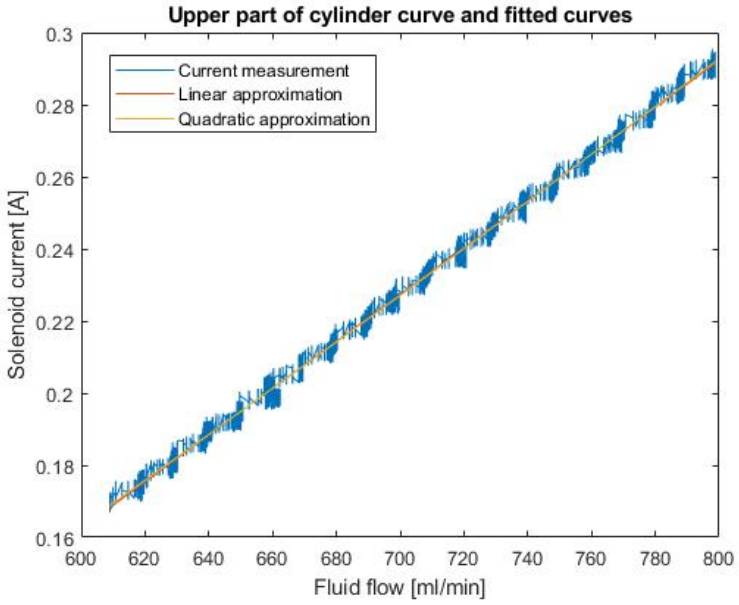

FIGURE 5.7: Fitted linear (red) and quadratic (yellow) curves along the upper part of current measurement for the cylinder float design in the third prototype.

In Figure 5.5 a linear and a quadratic approximation is done for the test using the

long cone float. As Figure 5.3 shows irregular behaviour at about 550-600 ml/min the data is divided into two three parts. Figure 5.6 is a linear and a quadratic approximation for the cylinder float in the lower range from 300 ml/min to 550 ml/min. Figure 5.7 shows approximations of the upper part of the plot, from 610 ml/min to 800 ml/min. The irregularity in the middle part is addressed in the coming analysis.

5.1.3 Analysis

The results from the first tests with the second prototype, Figure 5.1 and 5.2, shows that it exists a correlation between the fluid flow rate and the current applied to the solenoid, when maintaining equilibrium. While both a linear and a quadratic curve is fitted to the data, it is clearly seen that the quadratic curve follows the curve of the raw data. The linear approximation is, though not completely off, much less accurate. It is assumed that the correlation between the current and the fluid flow rate at this range can be approximated with a quadratic function.

As the second prototype only could operate at flow rates of 500 ml/min and above, the third prototype was designed with a smaller gap between the float and the tube. As a result the fluid flow could lift the float at around 200 ml/min. Tests presented in Figure 5.3 and 5.4 show that with the third prototype it is possible to measure the fluid flow rate in the desired range, between 300 ml/min to 800 ml/min. In Figure 5.3, however, an interesting phenomenon occurs. At a flow rate around 550 ml/min, the model shows some kind of transitional behaviour until it continues with a more linear shape, compare Figure 5.6 and 5.7. It is also noted that he current at the start of the upper part of the model, Figure 5.7, at approximately 600 ml/min is lower than the current at 550 ml/min flow, before the transition. The *phenomenon* of the transition is further discussed in Section 5.3.3.

Because of the observed transitional behaviour, the following tests are conducted using only the long cone float which shows a high potential in creating a model for the fluid flow measurement. The plot in Figure 5.5 shows the model between the current and the flow rate for the long cone in the third prototype. As in the previous model, the relation between fluid flow and solenoid current seems to be possible to approximate with a quadratic function. The proof of concept tests clearly shows that there exists a correlation, and that the new principle is possible to use. These tests are however conducted with the flow being controlled manually. An automated testing procedure is therefore introduced, to give a more coherent result in the measurements.

5.2 Test Automation

To create the models that the new flow sensor uses, the procedure from the tests for proof of concept is automated. A state machine is created to automate the Simulink model which controls the system. The state machine is designed to also conduct what is referred to as "loggings", i.e. tests that log relevant measurements over time. Also, the flow was feedback controlled with one of the two sensors used as reference.

5.2.1 Mappings

The mappings were made by alternating between two states. In the first state a reference for the fluid flow is set. That state is maintained until the flow has levelled out in accordance with a few constraints, namely maintained a flow within 2 ml/min from the reference flow for 3 seconds. After levelling out, the measuring state is entered. In the measuring state, the fluid flow measured by the electromagnetic flow sensor, and the solenoid current are logged in a data file. Along with these measurements, the pump control signal and pressures before and after the sensor are also logged in the data file. The measurements are logged over 5 seconds and the sampling frequency of the current measurement is $10^3 Hz$, providing 5000 data points at each fluid flow level. After the 5 seconds of measurement, the first state of setting a new reference is re-entered. The same procedure is then repeated until measurements have been made at the last fluid flow level of the mapping. By waiting for a steady flow before collecting any measurement data, the collected data is focused to steady state measurements, ignoring transitional measurements that might differ depending on the control of the flow and solenoid.

There are four different mapping sequences that can be initiated. One main mapping of the full spectrum of the flow and three partial mappings that focuses the mapping to a smaller area in which, also, smaller increments in the fluid flow are made. Furthermore, the measurement time in the partial models is doubled to 10 seconds. The specific ranges and step sizes are the following:

1. Range [ml/min]: 300-800, Step [ml/min]: 25, Measurement time [s]: 5
2. Range [ml/min]: 300-400, Step [ml/min]: 10, Measurement time [s]: 10
3. Range [ml/min]: 500-600, Step [ml/min]: 10, Measurement time [s]: 10
4. Range [ml/min]: 700-800, Step [ml/min]: 10, Measurement time [s]: 10

The results of the mappings are 21 focused steady state points in the full scale model and 11 points in the partial models. The points are then run through the same process of fitting functions to the acquired data as in the proof of concept tests. With the partial mappings, the model for fluid flow is more accurately approximated within their respective intervals. The loggings are made at constant fluid flow levels at the middle of these mappings. Mappings 2, 3 and 4 are created for accurate measurement at 350 ml/min, 550 ml/min and 750 ml/min respectively.

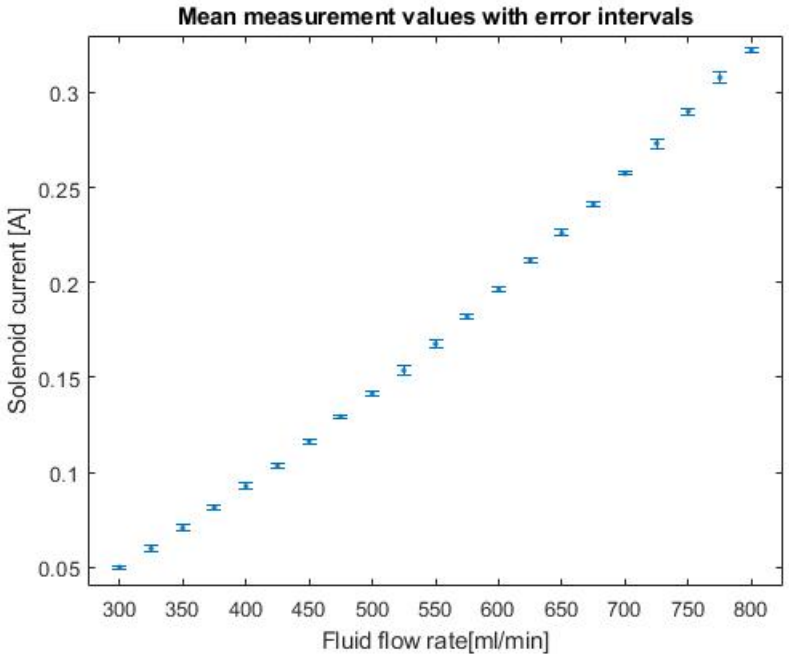

FIGURE 5.8: Plot of a mapping made with the automated system. Mean values at measurement points and 3σ intervals.

In figure 5.8, the plot of measurements from a full scale mapping is presented. The presented measurements are calculated mean currents at each flow and the error bars have the length of 3 standard deviations (σ) above and below the mean. The three σ errors correspond to the intervals in which the true value is found with a probability of 99.7%.

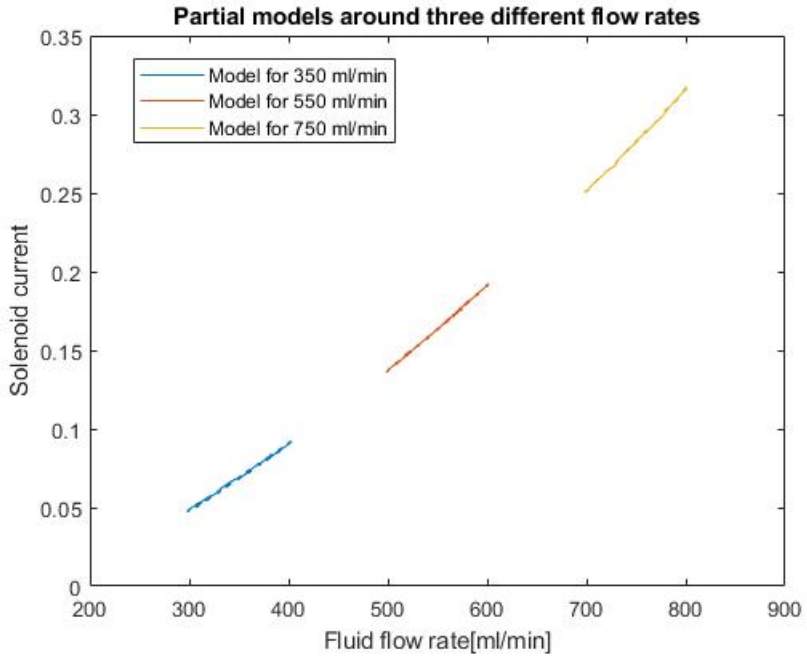

FIGURE 5.9: Partial models for testing at three different flow rates.

A plot of measurements from the three partial mappings is seen in Figure 5.9. The increment between the steps is 10 ml/min. Here, the raw data of the mappings is plotted.

The mappings serve two purposes. The first is giving a picture of how the drag force on the float changes with the fluid flow rate. A comparison made of the two mappings made at e.g. two different temperatures, can show how the temperature (or any chosen parameter) affects the model. The second purpose is the described model creation. The mappings are then inverted to have them describe a function from current to flow instead of the flow to current models shown above. A model of that type looks like the one seen in Figure 5.10 below.

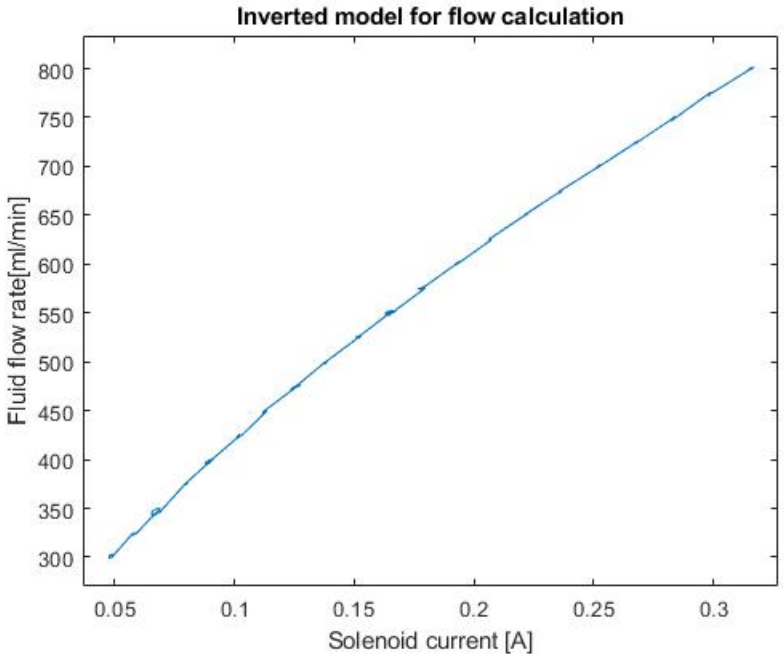

FIGURE 5.10: Plot of an inverted mapping.

5.2.2 Logging

The logging procedure is automated in order to produce more reliable results. The logging procedures can either be performed over a specific set time or with a different target, such as a target volume, but with an accurate time measurement. Synchronization of loggings with manual time measurement can result in a lot of errors due to human reaction times. That is the main reason for automating the logging.

In the loggings, data is gathered from both the electromagnetic flow sensor and the new sensor. For a concrete actual reference, the fluid flow is led to the reservoir on the scale. The scale reading provides the indisputable measurement of the total volume that has been passing through the system. To be able to compare the values of the scale to those of the two flow sensors, their measurements are integrated in the software. Along with the flow and volume measurements, the two measured pressures are logged to keep track of changes in pressure during the logging. From the program it is possible to set the desired flow rate, which sensor to operate from, and the desired target volume to aim for. The tests with the scale are conducted by controlling the pump with the measurement from the new sensor as actual value of the flow. When either 350 ml/min, 550 ml/min or 750 ml/min is set to be the desired flow rate its corresponding partial current model is used.

Prior to the test a specific target volume is set in the program. The test is initiated manually when the value readings have stabilised. When the test starts, a digital signal is transmitted to the relay, which activates and changes the fluid path to the reservoir on the scale instead of back to the circulation reservoir. The fluid path is changed by the

three-way valve. When the integrated value of the new sensor reaches the target volume, the relay is switched off and the flow path is set to direct the fluid back to the circulation reservoir.

When comparing results of the loggings the measurements of the new sensor, the electromagnetic flow sensor and the scale are analysed for their mean values, their standard deviation and their error relative the target volume. Thereby the tests assess the new sensors ability to measure the goal volume.

A last thing to note is that the scale measures mass and not volume. The volumes presented as measured by the scale are calculated volumes, based on the mass measurement of the scale and the density of water at the current temperature.

5.3 Accuracy and Precision

To test the accuracy and precision of the new sensor a series of loggings were made at each of the three flow levels, 350 ml/min, 550 ml/min and 750 ml/min. Each series consist of ten tests. Since the logging procedure is based on the new sensors measurement integrating up to 5000 ml the measured volume according to the new sensor is 5000 ml for each logging, with no deviations. Therefore, only the other two measurements are presented in plots and it is their deviation from 5000 ml that is analysed. For precision, the most significant part to study is the standard deviation of the results. For the accuracy, the difference between the mean values are the most interesting piece of information.

5.3.1 Results

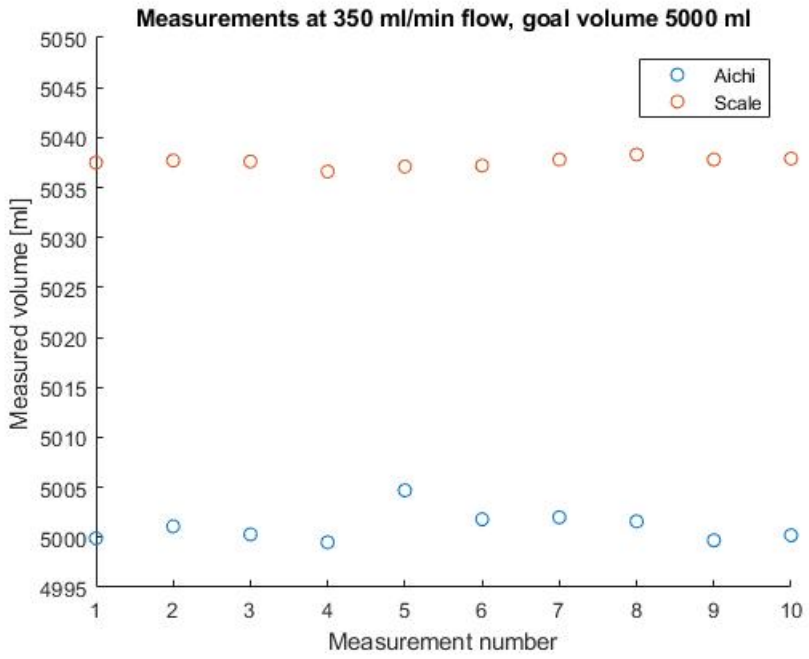

FIGURE 5.11: A scatter plot of integrated electromagnetic flow sensor measurement and volumes calculated from final scale readings. Ten measurements made at a flow rate of 350 ml/min.

TABLE 5.1: Mean values and standard deviation of ten tests at 350 ml/min flow.

Flow: 350 ml/min	*Mean [ml]*	*Standard deviation [ml]*
Electromagnetic	5001.08	1.56
Scale	5037.55	0.48

In Figure 5.11 the final volumes of the electromagnetic flow sensor and the scale from ten measurements are shown in a scatter plot. The fluid flow rate was 350 ml/min. The scatter plot shows the value reading for the electromagnetic flow sensor and the calculated volume from the scale values. Table 5.1 shows the mean value of the tests and the standard deviation for new sensor, the scale and the electromagnetic flow sensor. Test results for a flow rate of 550 ml/min are presented in Figure 5.12 and Table 5.2. In Figure 5.13 and Table 5.3 test results from flow rate of 750 ml/min are presented.

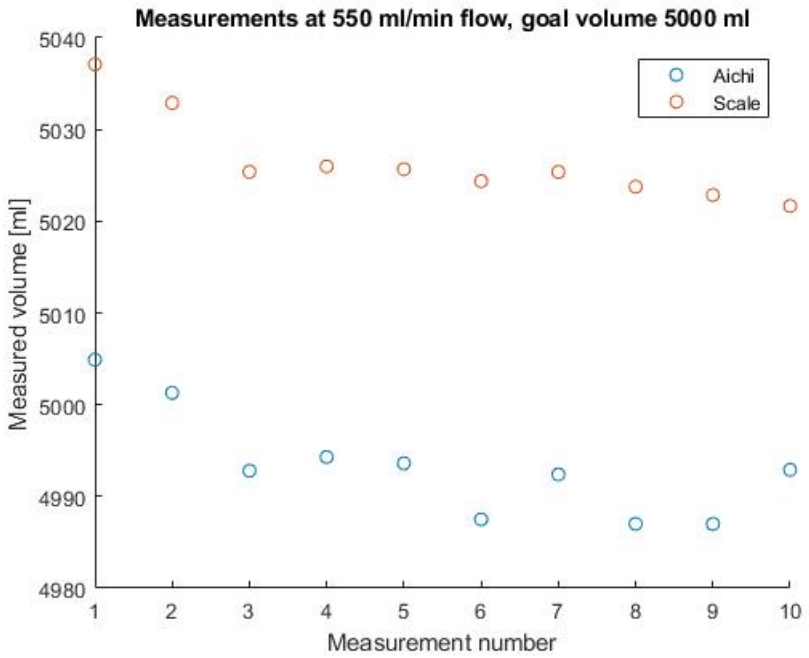

FIGURE 5.12: A scatter plot of integrated electromagnetic flow sensor measurement and volumes calculated from final scale readings. Ten measurements made at a flow rate of 550 ml/min.

TABLE 5.2: Mean values and standard deviation of ten tests at 550 ml/min flow.

Flow: 550 ml/min	*Mean [ml]*	*Standard deviation [ml]*
Electromagnetic	4993.37	5.91
Scale	5026.51	4.78

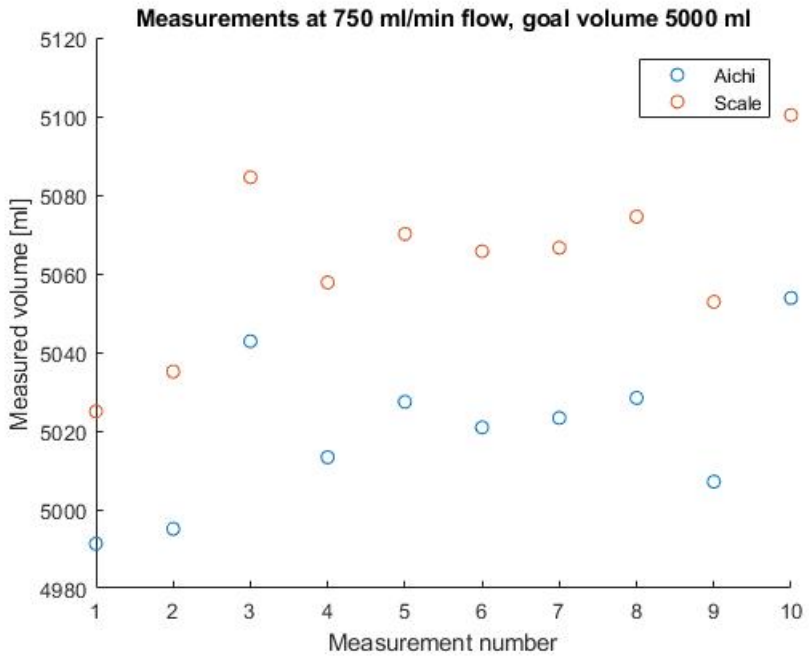

FIGURE 5.13: A scatter plot of integrated electromagnetic flow sensor measurement and volumes calculated from final scale readings. Ten measurements made at a flow rate of 750 ml/min.

TABLE 5.3: Mean values and standard deviation of ten tests at 750 ml/min flow.

Flow: 750 ml/min	*Mean [ml]*	*Standard deviation [ml]*
Electromagnetic	5020.34	19.59
Scale	5063.24	22.15

In Table 5.4 the mean value and standard deviation of the difference between the electromagnetic flow sensor and scale volumes are presented.

TABLE 5.4: Difference between integrated electromagnetic flow sensor value and volume calculated from final scale reading.

Difference Scale - Electromagnetic	*Mean [ml]*	*Standard deviation [ml]*
350 ml/min	36.47	1.66
550 ml/min	33.14	2.59
750 ml/min	42.90	3.84

5.3.2 Analysis

The analysis of the accuracy and precision is made separately to avoid a mix up.

Accuracy

High accuracy, can be described as the ability to measure the true value of a parameter. A good accuracy is seen as only small systematic errors in the measurements. As can be seen in the results, the mean accumulated volumes of the scale differ from the 5000 ml of the new sensor with between 26-63 ml. Since the new sensor is mapped to the flow measurement of the electromagnetic flow sensor, no better accuracy can be achieved for the new sensor than the one of the electromagnetic. Therefore, the difference between the electromagnetic sensor and the scale presented with mean values and standard deviations in Table 5.4 is interesting to look at.

At all three flow rates the electromagnetic flow sensor measures between 33 and 43 ml less than the scale. This indicates an offset between the real flow and the one measured by the electromagnetic sensor. As mentioned earlier, the electromagnetic sensor measurement is read by counting the number of pulses it creates per time unit. The number of pulses is then scaled with a volume specified by the provider of the sensor. An error in this volume create an offset in the measured flow and further on, an offset in the measured volume. Tuning this scaling parameter to the calculated scale value makes the electromagnetic sensor more accurate. Mapping the new sensor to the electromagnetic sensor measurement after that should provide a better accuracy for the new sensor.

Precision

Precision is the variation of random errors in measurements. A high precision provides small random errors which can be translated into a low variance or standard deviation. As the new sensors integrated value was the reference for when to stop the loggings it reaches 5000.00 ml each time. The analysis is then made of how well it connects to reality, i.e. the scale value. At 350 ml/min flow, the calculated volume from the scale measurement has a standard deviation of 0.48 ml. For a perfect normal distribution this would mean that the probability is 0.997 that a value is within $3 \cdot 0.48 = 1.44$ ml from the mean value. If the accuracy is improved, i.e. the offset is reduced, with a mean volume of 5000.0 ml there is a 99.7% probability to have a relative error less than 0.288 $\%_{oo}$. This shows a good precision in volume measurement at the flow rate of 350 ml/min. It is worth to mention though, that there is not quite enough tests performed to prove that the random errors follow a normal distribution. The same calculations as presented for 350 ml/min flow are summarized in Table 5.5 below.

TABLE 5.5: Statistical calculations of relative error

Scale measurement at different flow rates	*Mean [ml]*	*Standard deviation (tripled value) [ml]*	*99.7% certain relative error [‰]*
350 ml/min	5037.55	0.48 (1.44)	0.288
550 ml/min	5026.51	4.78 (14.34)	2.868
750 ml/min	5063.24	22.15 (66.45)	13.290

The precision decreases with higher flow rate. The decreasing precision may be explained by the time constant of the system, which changes with flow. To analyse the time constant the magnitude of the forces are of interest. The force of gravity (5.1) and buoyancy (5.2) are constant when the flow increases.

$$F_g = mg = 0.00151 \cdot 9.81 \cdot = 14.8mN \tag{5.1}$$

$$F_{b@23^\circ C} = \rho_{fluid} g V = 997.5 \cdot 9.81 \cdot 0.808e10^{-6} = 7.9mN \tag{5.2}$$

At worst case the float is not affected by any magnetic force between two samples. In this case, the resultant force acting on the float is the same as the magnetic force needed to hold the float at a fixed position. Studying Figure 5.9 the approximated current needed to hold the float can be determined. Comparing this current with tests in Appendix A the magnetic force can be approximated. The approximated resultant force at 350 ml/min and 750 ml/min are presented in Table 5.6. The mass of the float is approximately 1.5 g. With the resultant force and the mass known the acceleration of the system, when no current is applied to the solenoid, can be calculated by $a = \frac{F_r}{m}$. Where a is the acceleration, F_r is the resultant force on the float and m is the mass of the float. Table 5.6 also presents the approximated acceleration at 350 ml/min and 750 ml/min.

TABLE 5.6: Approximated resultant force and acceleration of the float.

	Resultant Force $[mN]$	Acceleration $[m/s^2]$
350 ml/min	32	21
750 ml/min	96	64

The system samples the position with a constant frequency of 1 kHz, the increase of the acceleration can be a reason why the precision is better at lower flow. Between the samplings period the float can travel 3 three time longer distance if no current is applied to the solenoid. The distance the float travels between samples may affect how smooth the position control is. If the distance travelled between two samples is too long, the controller has a problem reacting to the change in position.

The acceleration at 750 ml/min in Table 5.6 would achieve a velocity of 0.0064 m/s from 0 m/s during one sample. The mean velocity over the sample period is then 0.032 m/s and the distance travelled is subsequently 0.032 mm. If the system samples with a higher frequency the distance the float can travel between two samples decreases. This can lead to better precision at higher flow rates.

Another factor might be the relation between the signal of Hall effect sensor and its distance to the permanent magnet. The relation is logarithmic, which makes the position control less sensitive to movement far away. The signal only really increases notably when the magnet is only a few centimetres away. The signal variation around the operating point is large. A small position change will then cause a large change in position measurement. The combination of the logarithmic signal and the distance travelled between samples might, in combination, can make the system less stable.

5.3.3 Phenomenon

Test in proof of concept, Section 5.1.2 Figure 5.3, the phenomenon is first observed. This phenomenon is further investigated, since it has a large effect on the measurements. The phenomenon first occurred with the cylindrical float at a certain flow. When the test rig was upgraded with the three-way valve the phenomenon occurred also for the long cone float. It was believed that the three-way valve increased the absolute pressure in the system. This led to more investigation of the system to determine when the phenomenon occurs.

In Figure 5.14 the cylinder is used to investigate the phenomenon. It is seen that the model fluctuate between two models, one low model and one high. At lower flow rate the model follows the higher model.

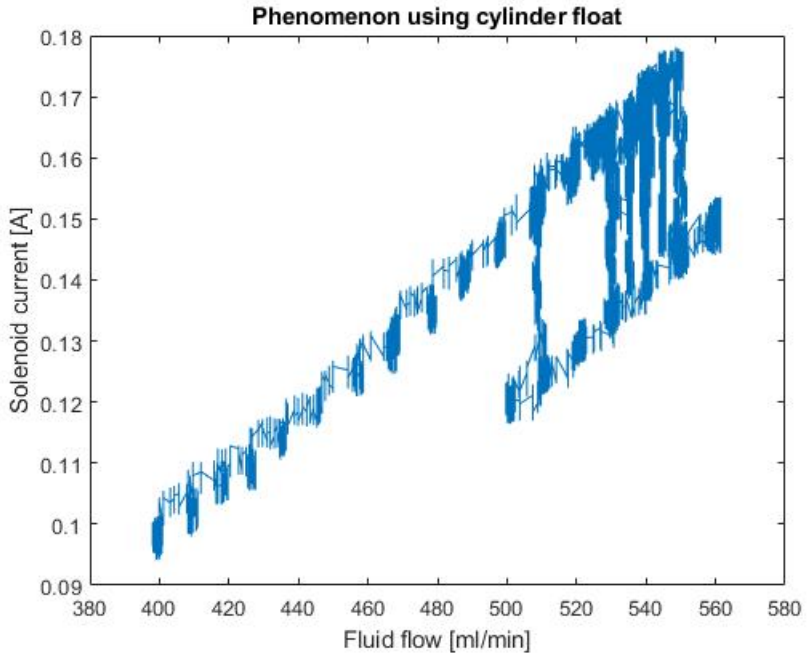

FIGURE 5.14: Current measurement using the cylindrical float at flow rates where the phenomenon occurs.

Phenomenon Investigation

To analyse the behaviour of the fluid flow further, the Reynolds number for the flow is calculated. Reynolds number can be used to analyse if the flow is laminar or turbulent. In the flow theory presented in [4], Reynolds number can be calculated in a rotameter by using Equation (2.9) in Section 2.4.2. In Figure 5.15 a plot for Reynolds number is illustrated.

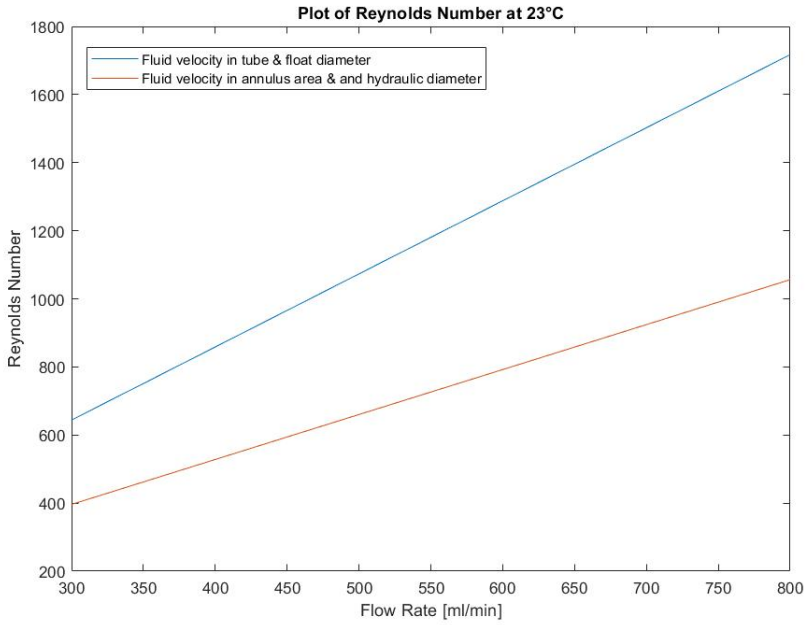

FIGURE 5.15: Calculation of Reynolds number along the range of flows in tests. The two plots are results of two different calculation methods

As mentioned in the theory chapter, Chapter 2, there are two possible methods to calculate $Re = \frac{Ud}{\nu}$. One uses the diameter of the tube (d_{Tube}) for velocity calculation and the diameter of the float (d_{float}) inserted as d. The second uses the hydraulic diameter ($d_h = d_{tube} - d_{float}$) for both velocity calculation and insertion in d, Section 2.4.1. Both methods are plotted, the first in blue and the second in red. It is seen that the Reynolds number calculated with the first method reaches the transition area between laminar and turbulent flow at just below 500 ml/min. The first method is the one said to be best used for rotameters according to [4]. As the new sensor has a different shape of the tube, it might be less accurate. With that said, the phenomenon could possibly be a transition from laminar to turbulent flow.

One other explanation might be that the float might starts to wobble or spin, which results to the boundary layers achieving a different behaviour. However, a laminar/turbulent transition is the working hypothesis regarding the phenomenon.

5.4 Pressure

Testing the effect of pressure differences has two aspects. The first is a general pressure dependency. In the theory, the pressure is not explicitly included as a variable affecting the dynamics of the system. Relative pressure to the atmosphere is generally not relevant to know regarding flow of incompressible fluids. Some of the fluid parameters might change enough due to pressure changes to affect the model. The second aspect of pressure dependency is how a high pressure affects the new sensor itself. It is recommended by Baxter employees to test the performance at 1 bar of relative pressure.

Two methods were used when testing the effect of different levels of pressure in the system. To get a first view of how the model would change due to a higher pressure mappings were made at a different starting pressures.

To further analyse the system, 20 loggings were made at low and high pressure for each of the three flow levels, 10 loggings at each pressure and flow level. During both high and low pressure tests the models used were created at low pressure. The low pressure results is then seen as reference measurements. The high pressure measurements are then analysed to see how well the low pressure model works at high pressure.

The overall pressure level in the system was set by turning the trim valve. The pressure referenced is the lower of the measured pressures, the one after the new sensor. For each logging, the pressure is determined as the mean pressure during the logging.

5.4.1 Results

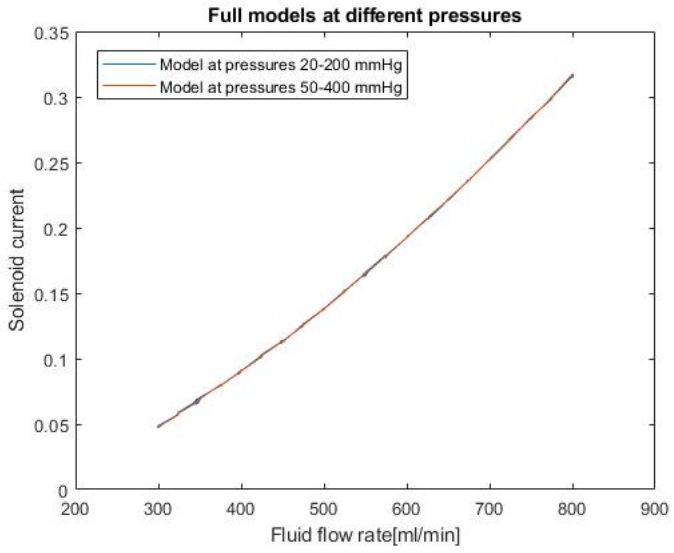

FIGURE 5.16: Plot of two mappings at different pressures.

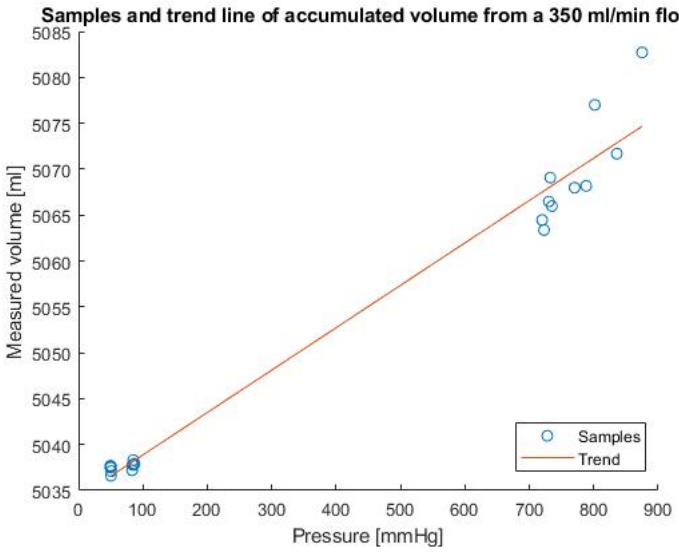

FIGURE 5.17: A scatter plot of volumes calculated from final scale readings and trend line with respect to pressure. Ten measurements made at low pressure a flow rate of 350 ml/min. Ten measurements made at high pressure and same flow rate.

Figure 5.16 presents two mappings at different pressures during the sequences. Figure 5.17 shows a scatter plot of volumes calculated from scale measurements of 20 loggings at 350 ml/min flow. Also, the Figure shows a line created from a linear regression of the relation between volume and relative pressure. Table 5.7 below shows the linear model along with intervals of confidence for the linear and constant term.

TABLE 5.7: Linear regression for the measured volumes depencency on the pressure @ 350 ml/min

Linear regression V(P) @ 350 ml/min	*Value*	*Intervals of confidence (95%)*
k	0.0462	(0.0424, 0.0500)
m	5034	(5032, 5036)

Table 5.8 shows the mean values, standard deviation and the relative error in the mean values, of the three different measurement methods at the two pressure levels. All of the for a flow with a reference of 350 ml/min.

TABLE 5.8: Mean measurements and standard deviations of the the three measurement alternatives for loggings at 350 ml/min. The relative errors are presented as the per mille deviation from 5000 ml.

Sensor	*Mean [ml]*	*Standard deviation [ml]*	*Relative error comp. New sensor [‰]*
350 ml/min flow at reference pressure			
Electromagnetic	5001.08	1.56	0.22
Scale	5037.55	0.48	7.51
350 ml/min flow at high pressure			
Electromagnetic	5028.72	6.13	5.74
Scale	5069.69	6.00	13.94

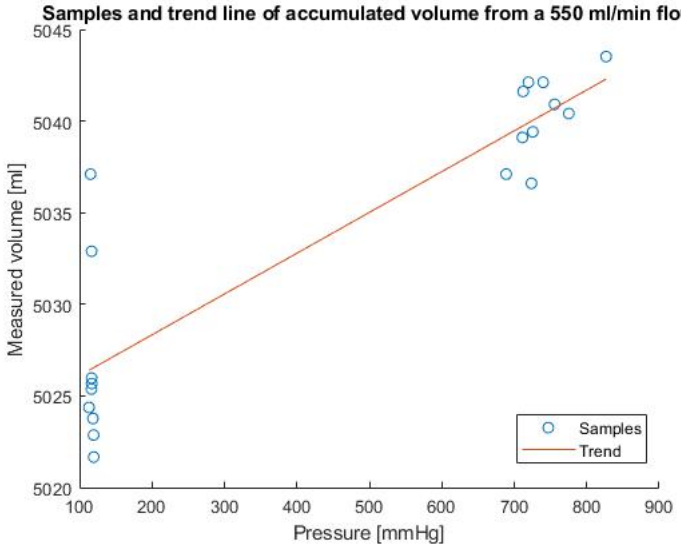

FIGURE 5.18: A scatter plot of volumes calculated from final scale readings and trend line with respect to pressure. Ten measurements made at low pressure a flow rate of 550 ml/min. Ten measurements made at high pressure and same flow rate.

Figure 5.18 shows a scatter plot and linear regression line of volumes calculated from scale measurements of twenty loggings at 550 ml/min flow. Table 5.9 below shows the linear model and the parameters respective intervals of confidence. Mean values, standard deviation and relative errors for the 550 ml/min loggings are presented in Table 5.10.

TABLE 5.9: Linear regression for the measured volumes depencency on the pressure @ 550 ml/min

Linear regression V(P) @ 550 ml/min	*Value*	*Intervals of confidence (95%)*
k	0.0223	(0.0168, 0.0277)
m	5024	(5021, 5027)

TABLE 5.10: Mean measurements and standard deviations of the the three measurement alternatives for loggings at 550 ml/min. The relative errors are presented as the per mille deviation from 5000 ml.

Sensor	*Mean [ml]*	*Standard deviation [ml]*	*Relative error comp. New sensor [‰]*
550 ml/min flow at reference pressure			
Electromagnetic	4993.37	5.91	-1.33
Scale	5026.51	4.78	5.30
550 ml/min flow at high pressure			
Electromagnetic	5001.57	2.33	0.31
Scale	5040.29	2.24	8.06

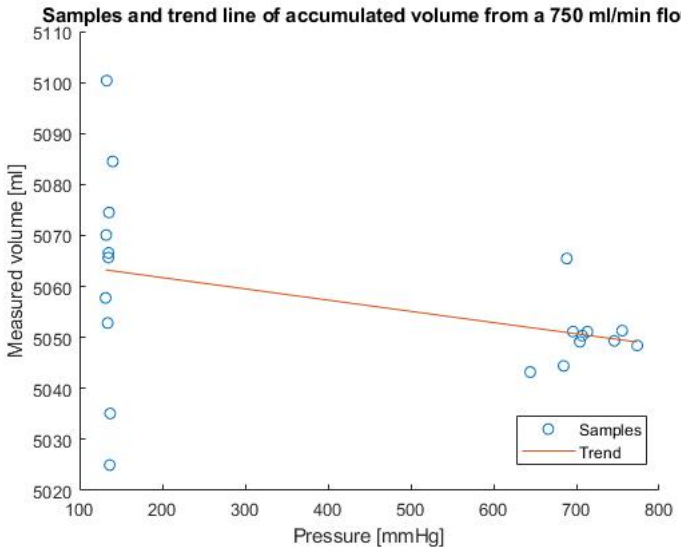

FIGURE 5.19: A scatter plot of volumes calculated from final scale readings and trend line with respect to pressure. Ten measurements made at low pressure a flow rate of 750 ml/min. Ten measurements made at high pressure and same flow rate.

Figure 5.19 shows the scatter plot and linear regression of twenty 5000 ml loggings at 750 ml/min. In Table 5.11 the properties of the linear model are presented. In Table

5.12 the mean measurements, standard deviations and relative errors of each sensor are presented.

TABLE 5.11: Linear regression for the measured volumes depencency on the pressure @ 750 ml/min

Linear regression V(P) @ 750 ml/min	*Value*	*Intervals of confidence (95%)*
k	-0.0220	(-0.0484, 0.0043)
m	5066	(5053, 5080)

TABLE 5.12: Mean measurements and standard deviations of the the three measurement alternatives for loggings at 750 ml/min. The relative errors are presented as the per mille deviation from 5000 ml.

Sensor	*Mean [ml]*	*Standard deviation [ml]*	*Relative error comp. New sensor [‰]*
750 ml/min flow at reference pressure			
Electromagnetic	5020.34	19.59	4.07
Scale	5063.24	22.15	12.65
750 ml/min flow at high pressure			
Electromagnetic	5003.34	5.36	0.67
Scale	5050.34	5.99	10.08

5.4.2 Analysis

From the model variation at different pressures, Figure 5.16, not too much can be said. At low fluid flow rates, the pressure difference is very small and was therefore never likely to show any difference. At the higher flow rates, the pressure gets relatively much higher, but still show only little to no change in the model.

The difficulties with testing mappings at different pressures, and especially higher pressures, is the variation of pressure as the mapping is performed. At each change of flow rate, the pressure increases past the level that would be maintained for constant flow at that rate. The system is not able to hold together for much higher pressures than what is tested in the loggings. The change of pressure that is needed to see a change in the model at low flow, early in the mapping, would cause the new sensor to pop open in the ends at a rise in the flow rate.

Because of this situation, focus of the pressure testing was kept at analysing the loggings. From the model tests, there can at least be said that there is no big pressure dependence seen.

The loggings show some signs of a pressure dependency. Both the 350 and 550 ml/min loggings (Figures 5.17 and 5.18) show a trend in an increased volume on the scale while still measuring 5000 ml with the new sensor. This indicates a lower flow rate measurement by the new sensor than what is measured at lower pressures. Both

linear regressions show a positive relation between increased pressure and accumulated volume on the scale (decreased measurement by the new sensor).

In the 750 ml/min scatter, Figure 5.19, the trend instead has a negative incline with increasing pressure. The interval of confidence for the k-value (see Table 5.11) does covers zero, though. Therefore, it can not be shown with a 95% certainty that the pressure has an impact at 750 ml/min.

However, the loggings at lower pressure for 750 ml/min did show some "fluctuations" so to say. As in the case of the measurements when experiencing the phenomenon, the measurement suddenly dropped to a lower level one or more times over most of the loggings. The two lowest points in the left half of the scatter show the measurements of loggings where none or only one "fluctuation" occurred. Had these measurements had a higher representation in the linear regression, the same pressure dependency as in the two earlier cases might have been seen.

Connections between the yielded results and theory regarding the effect of pressure is not easy too see, or any less to prove. According to the theory found on the rotameter flow equation and other studied flow theory, the pressure should (under these circumstances) not show a considerable effect. Therefore the results and the theory is, shortly put, not coherent.

A possible explanation for the gathered results might be small tensions in the tube of the new sensor. The stresses in the tube at high pressure might be enough to achieve a small increase in the inner diameter. With a larger tube the drag force decreases, as in the case of the rotameter. A weaker drag force would require a lower magnet force to maintain the given position of the float. The weaker magnetic force and subsequently weaker solenoid current would thereby result in a lower measured flow.

5.5 Temperature

Fluid density and viscosity are two parameters that are included in the theory of the forces affecting the float. As both of the two are temperature dependent, tests of model changes at different temperatures are of interest.

The results of the temperature tests are presented similarly to the pressure tests. The already noticed, strong temperature dependency shifted the tests a little bit. Several mapping tests at different temperatures were conducted to get a better picture of model changes due to temperature. As for logging tests, the "fluctuations" at higher flows causes the temperature loggings to be kept at lower flows (350 and 550 ml/min). The combination of good mapping results and the long test times of 350 ml/min tests causes the loggings to be focused to 550 ml/min loggings. The reason longer tests are rejected is the time dependent temperature changes in the reservoirs.

At temperatures further from room temperature than 23°C there are stationary errors in the temperature control. As the volume in the circulation reservoir decreases, the error decreases as well, since there is a smaller mass to control. This creates a change in water temperature over time. Reducing the test duration is seen as the best available way to eliminate errors due to this behaviour. The quickest available tests is therefore seen as sufficient for logging tests. During the loggings, the model used is always the model created at 23°C. The test results are then analysed from the angle of how big errors occur due to deviations from the model temperature.

5.5.1 Results

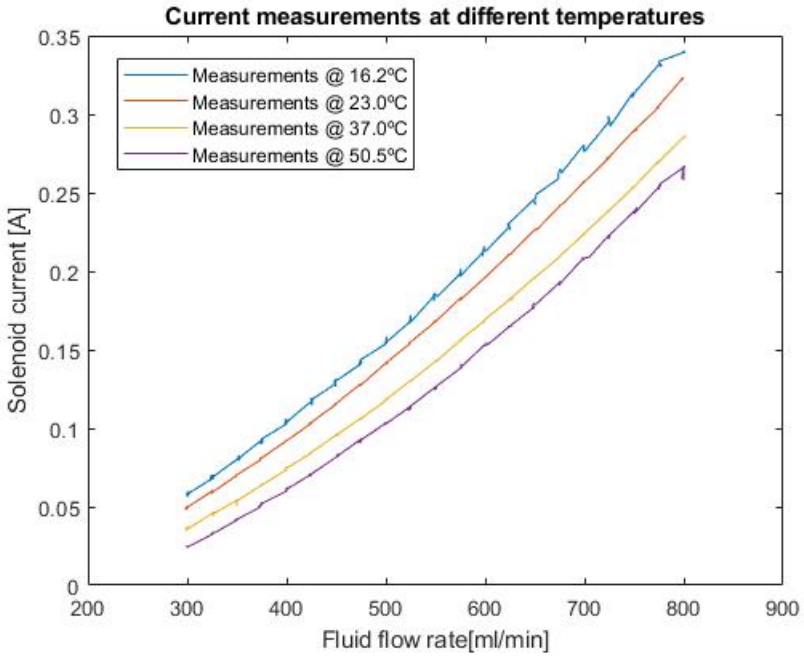

FIGURE 5.20: Plot of four mappings of current versus fluid flow at four different temperatures.

In Figure 5.20 the plots of measurements from four mappings at different temperatures are presented. In the 16.2°C mapping a quick decline in the current derivative can be seen. This is due to that the maximum current available with the 24 V supplied is reached. The final point of measurement in the 16.2°C model should therefore be neglected. In the model created from that mapping, the last point of measurement is not used.

TABLE 5.13: Mean values of measurements, standard deviation and relative errors @ 23°C and 37°C

Sensor	*Mean [ml]*	*Standard deviation [ml]*	*Relative error comp. New sensor [‰]*
Logging @ 23°C, 550 ml/min			
Electromagnetic	4993.37	5.91	-1.33
Scale	5026.51	4.78	5.30
Logging @ 37°C, 550 ml/min			
Electromagnetic	5341.05	16.89	68.21
Scale	5409.73	17.39	81.95

In Table 5.13, the measurements of loggings at 23°C and 37°C are presented with mean values, standard deviation and error relative to the target volume. In Figure 5.21

plots of the approximated models of current vs. flow relation at the tested temperatures are presented.

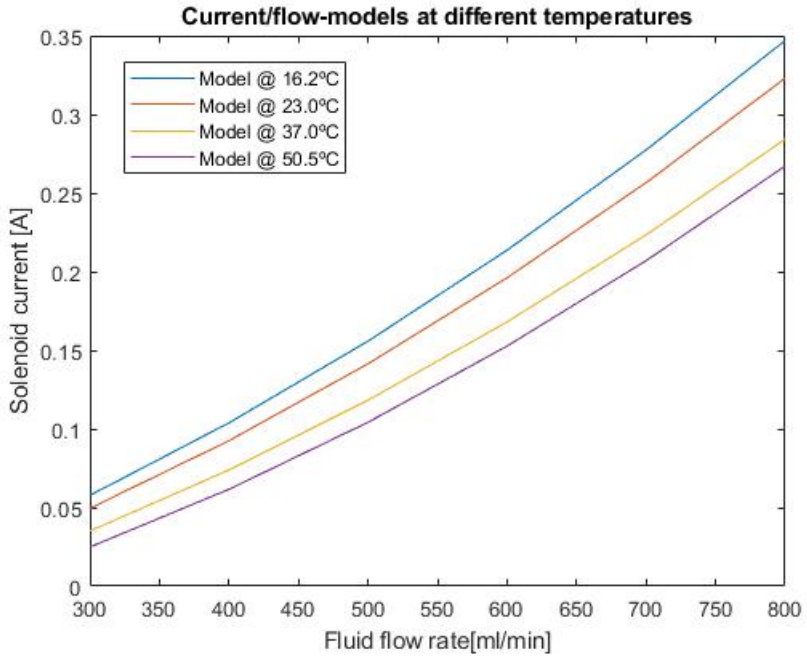

FIGURE 5.21: Plot of four models of current versus fluid flow at four different temperatures.

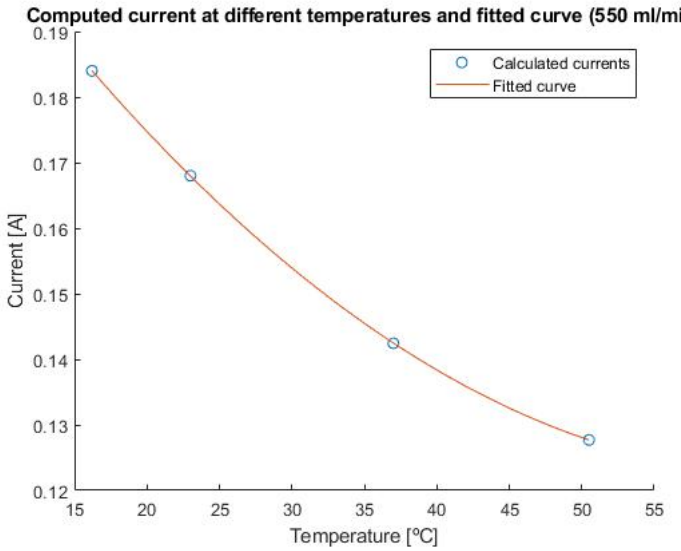

FIGURE 5.22: Scatter plot of four points in the current versus fluid flow model at four different temperatures. A fitted curve shows an approximated relation between solenoid current and temperature at a flow of 550 ml/min.

In Figure 5.22 the four models values of electric current at the flow rate used for logging testing are plotted against the temperature. The numerical values and their respective percentual deviation from the reference value at 23ºC are presented below in Table 5.14.

TABLE 5.14: Numerical values of current magnitude at four different temperatures and constant flow.

Temperature	*Current [A] @ 550 ml/min*	*Deviation from current @ 23.0ºC [%]*
16.2ºC	0.1840	9.52
23.0ºC	0.1680	0.00
37.0ºC	0.1424	-15.21
50.5ºC	0.1277	-23.99

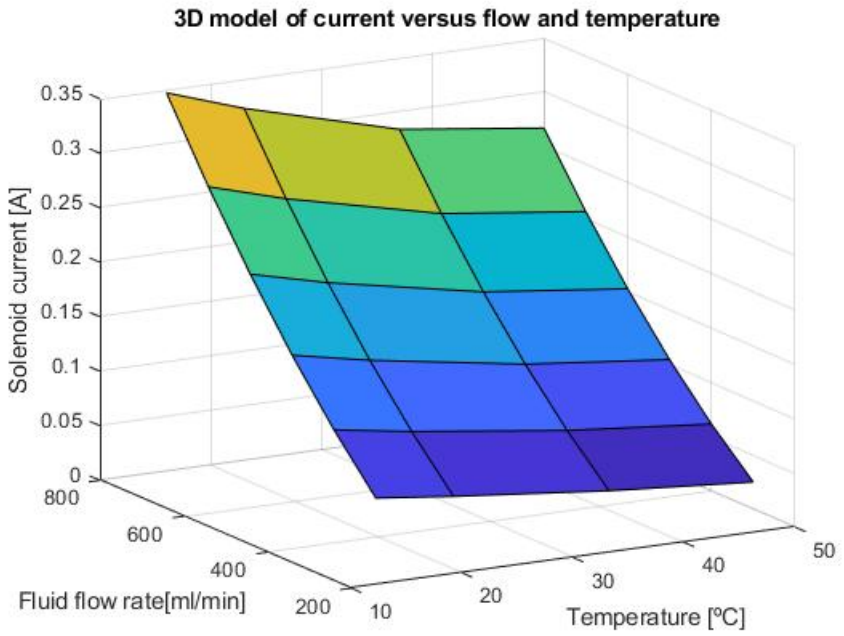

FIGURE 5.23: 3D surface plot of current dependency of flow and temperature.

Finally, a 3D-plot was created to visualise how a model with temperature correction could look. In Figure 5.23 a surface plot of the current vs. flow and temperature is shown.

5.5.2 High Temperature Cleaning

When water is standing still in a system over some time, biofilm appears inside the tubes. The biofilm affects the system and needs to be cleaned with citric acid and warm water. The water needs to be around 85 degrees Celsius. At this temperatures magnetisations of permanent magnets can decrease in strength. Consequently, the effect of temporary high temperatures in the system needs to be analysed.

A cleaning procedure was performed to remove any biofilm in the system. After the cleaning procedure no observation was made that the high temperature had affected the permanent magnets strength.

5.5.3 Analysis

Studying the mappings and the models created from them, it is seen that with a lower temperature, the solenoid current required for the magnet to keep the float in place is increased. This is further strengthened by the fact that the volume measured by the scale (see Table 5.13) increases with the increasing temperature. The lower current needed at higher temperature causes the new sensor to measure a too low flow rate and has the system pump through almost an additional 10% before its integrated measurement reaches 5000 ml.

In Table 5.15 the buoyancy force for 0°C and 80°C are presented. As seen, the force differs by no more than 0.2226 mN. The lowest measured current in a test is about 0.02 A at 300 ml/min and 50.5°C. That current results in approximately 4.4 mN based on magnetic force experiments in Appendix A. The whole difference in buoyancy is just above 5% of that lowest measured magnetic force. Therefore, the buoyancy force is, within the current realistic frame, considered constant. Our tests only cover half the span of the temperatures, and the temperature span with the most rapid changes is not covered by our test span.

TABLE 5.15: Variation of buoyancy force between 0°C and 80°C.

Temperature [°C]	**Force [mN]**
0	7.924
80	7.7014

In Section 3.3.1 regarding the design of the float, one hypothesis was that with a certain float shape the C_D remains constant when Reynolds number changes. In Table 5.16 the deviation of drag force with a constant C_D and a constant flow rate of 550 ml/min is calculated with the approximated drag force Equation (2.7). The only changing parameter in the calculations is the density. Since the gravitational force (5.1) is constant and changes in buoyancy force (5.2) is insignificant, the current is proportional to the drag force and changes should therefore be proportional. Comparing the percentage calculated deviations in Table 5.16 with the measured deviations in Table 5.14 it is seen that the deviation is not the same, hence C_D can not be constant. Equation (2.11) for flow in rotameter also states that the flow is highly dependent of C_D.

TABLE 5.16: Deviation of drag force, constant C_D

Temperature [°C]	***Deviation from Drag Force 23°C, 550 ml/min [%]***
16	0.13
37	-0.42
50	-0.95

Before going into the process of calculating C_D an alternate route is presented. The four current/flow-models, in Figure 5.21, show the well known concept of mapping the current measured to a fluid flow. The same way, the Figure 5.22 shows a simple mapping between the temperature and the current. With a lot of current/temperature maps of this kind, a three dimensional map, a look up table, can be created to measure both temperature and current to get the fluid flow. The 3D-plot in Figure 5.23 shows a coarse 3D-mapping of the current measured at a known temperature and a known fluid flow. This can be inverted just like the 2D-mappings to calculate fluid flow as a function of current and temperature. An inverted 3D-mapping is shown below in Figure 5.24.

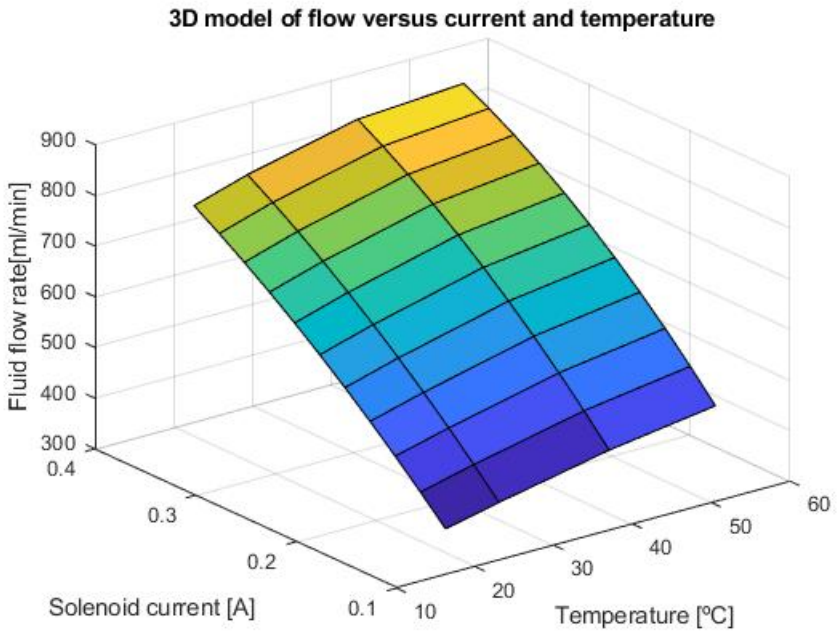

FIGURE 5.24: Inverted 3D surface plot of fluid flow dependency of solenoid current and fluid temperature.

Simulation of Drag Coefficient

As C_D is found to be varying with the temperature, the calculations of the drag force become a lot more complicated. Since C_D is determined experimentally for each specific case according to all theory found on the subject, there is no really strong theory to compare with when C_D is determined not to be constant. The further analysis tries to determine how C_D varies with the fluid flow.

The temperature affects the fluids properties significantly. In Figure 2.5 in Section 2.4.3 it is seen how rapid the kinematic viscosity decreases with a higher temperature, while the density only decreases slightly.

In Equation (2.9) for Reynolds number the kinematic viscosity appears. Reynolds number in the tube for the flow range between 300 ml/min to 800 ml/min, for different temperatures is seen in Figure 5.25

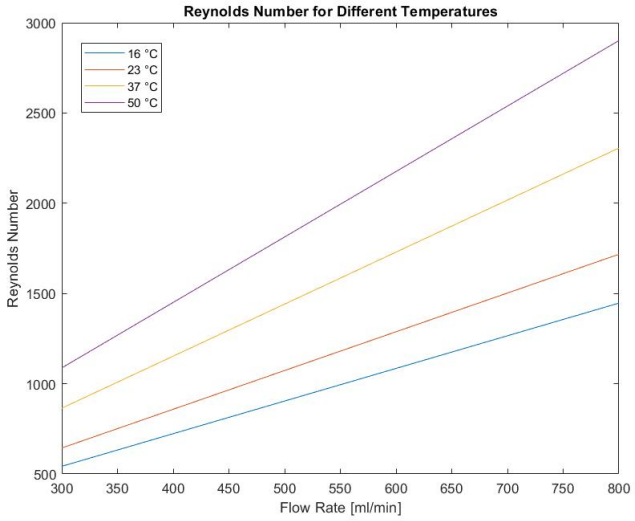

FIGURE 5.25: Calculation of Reynolds number through the four mappings at 16°C, 23°C , 37°C and 50°C

Figure 5.25 shows how Reynolds number increases with higher temperatures, this is due to a decrease in the the kinematic viscosity. Figure 2.4 in Section 2.4.2 shows experimented drag coefficient for different bodies. It is clearly seen that Reynolds number affects the magnitude of the drag coefficient. It is of interest to study how the drag coefficient changes with different temperatures.

To analyse the drag coefficient, the equations from Chapter 2 and data from Figure 5.20 are used. The analysis is based on the force equilibrium of gravity, buoyancy, drag force and magnetic force, $F_g + F_b + F_d + F_m = 0$, that needs to be fulfilled. Some of the parameters to the forces remains constant when the temperature changes, these parameters are held fixed while the program alter the drag coefficient to match results from experiments.

$$F_d(C_D) = C_D \frac{\rho U^2}{2} A \tag{5.3}$$

$$F_m = CI \tag{5.4}$$

$$I(C_D) = \frac{-F_d(C_D) - F_b - F_g}{C} \tag{5.5}$$

The magnetic force can be simplified to Equation (5.4) in the analysis since the parameters represented by the constant C do not change. Experiments in Appendix A are used to calculate an approximation of the constant to $C \approx -0.3082$ (negative due to orientation). Expression (5.2), as explained earlier is considered constant, while gravity, (5.1) remains completely constant. The drag force is assumed to be calculated as a function of C_D with Equation (5.3), but C_D is unknown.

To approximate C_D, Equation (5.5) is used. The electric current is, with this approximation, calculated as a function of C_D. C_D is then increased until the calculated current matches the current from experimental data from Figure 5.20. At each specific flow rate all other parameters such as the velocity, U, and density, ρ, are held constant. The program calculates C_D for the four temperatures, see Figure 5.26. The same program is used to calculate C_D when the velocity and Reynolds number are calculated according to hydraulic diameter in Section 2.4.1. The resulting, alternative C_D is plotted in Figure 5.27.

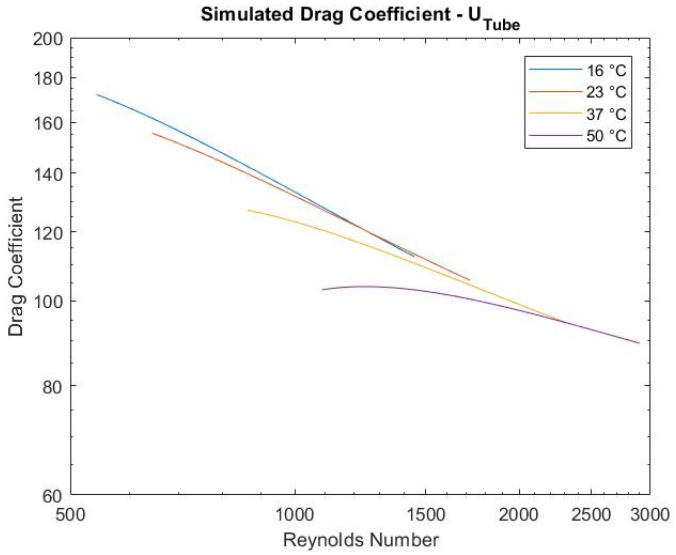

FIGURE 5.26: Simulated Drag Coefficient, simulated with velocity and Reynolds number of the fluid in the tube.

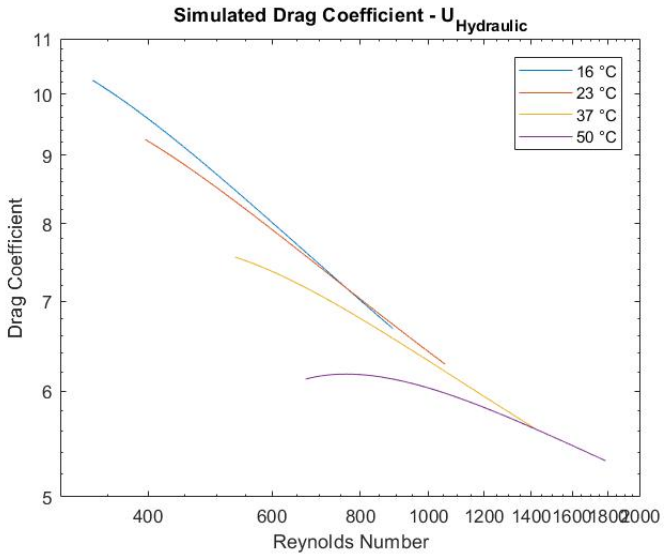

FIGURE 5.27: Simulated drag coefficient, simulated with the velocity and Reynolds number of the hydraulic diameter between the float and the tube.

In Figure 5.26 and 5.27 the graph tends to follow the same trend. With more experiments and more research of the flow equations, it might be possible to create a model for the temperature by studying C_D for specific Reynolds numbers. With a model of the temperature impact, the sensor can compensate for temperature changes, if a thermometer is implemented to the sensor. With a known temperature the viscosity can be determined and Reynolds number can be calculated. With a model C_D can be determined when Reynolds number is determined.

When velocity and Reynolds number is calculated using the hydraulic diameter, the drag coefficient decreases. The drag coefficients in Figure 5.27 seems more reasonable when considering drag coefficients in Figure 2.4, since the magnitude of C_D is similar.

5.6 Tilt

The new sensor is based on the principle of a rotameter. A rotameter is dependent on both the gravity force and the buoyancy, hence it must be placed in a vertical position. Since the new sensor has an additional force, the magnetic force, it is not fully dependent of gravity, as an ordinary rotameter.

The tilt decreases the resulting force in the direction of the flow, between the buoyancy and the force of gravity with a factor $\cos\theta$. Therefore, a tilted sensor should require a higher current to hold the float for the same flow rate, as simulated in Figure 5.28.

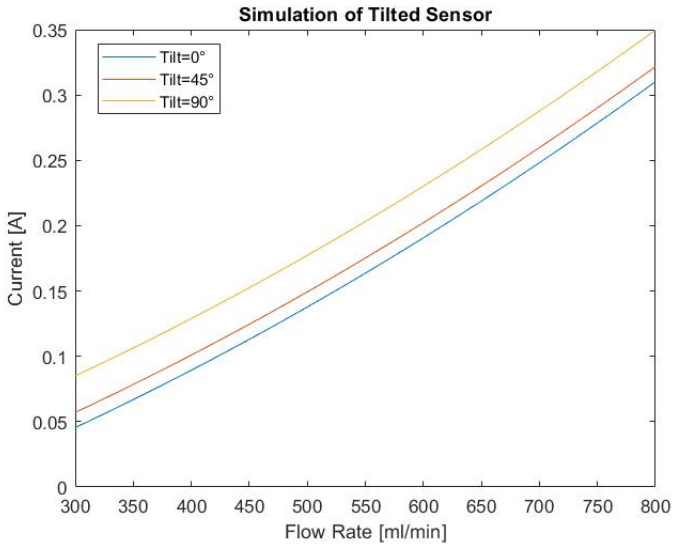

FIGURE 5.28: Simulated models for tilted sensor.

To analyse how tilt affects the sensor a series of mappings were performed. Foremost to see if the measurements would match the simulations. However, before analysing the effect of tilt around the horizontal axis, tests were conducted to see if rotation around the centre axis would give different results when the sensor is tilted. The Hall effect sensors measuring the position of the float are mounted on one side of the new flow sensor, a tilted sensor forces the float either closer to or farther from the Hall effect sensor due to gravity.

For Baxter's HD machines the maximum allowed tilt of the floor is 5º. Therefore, a worst case of 5º is tested. To get a sense of how larger angles affect the sensor, 45º and 90º is also tested.

5.6.1 Results

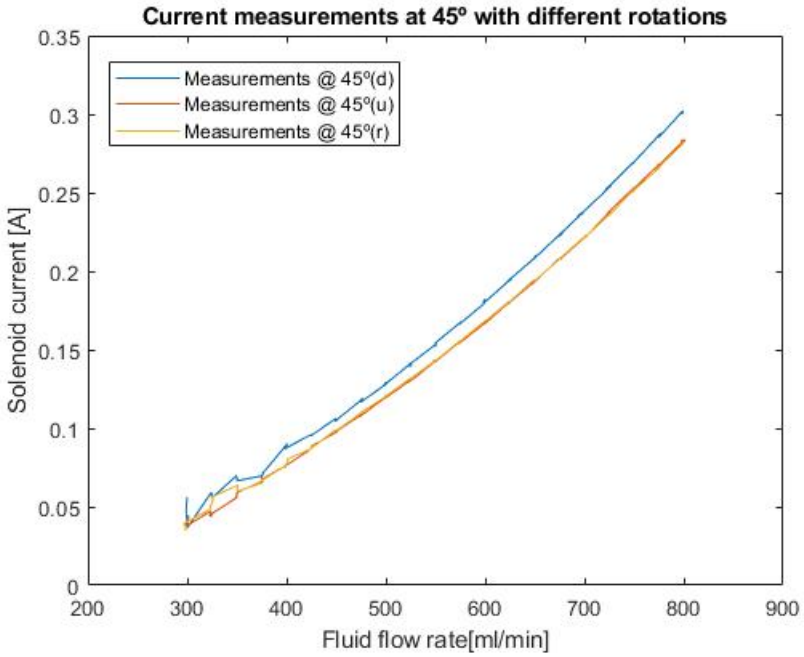

FIGURE 5.29: Plot of mappings at 45º angle with different orientations of the Hall effect sensor. 'd' for *down*, 'u' for *up* and 'r' for *right*.

In figure 5.29 three different current measurements from mappings at 45º are plotted for different orientations of the Hall effect sensors. The blue line is measured current with the Hall effect sensors placed below the tube ('d' for 'down'). The red and yellow lines are measurements from Hall effect sensor orientation *up* (u) and to the *right* (r) respectively.

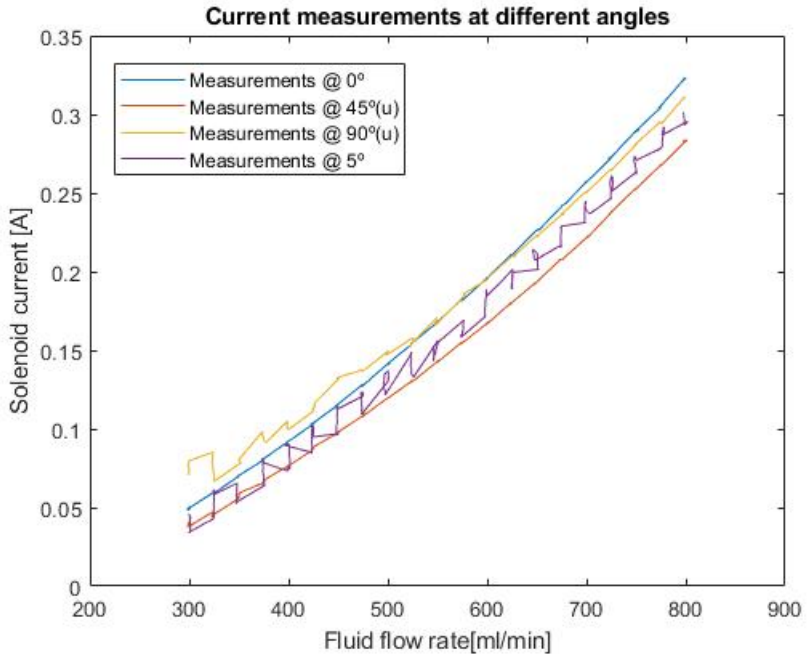

FIGURE 5.30: Plot of mappings at four different angles. A vertical mapping for reference, a 45° and a 90° angle mapping to see large tilt effect. 5° angle mapping to see behaviour at worst case.

In Figure 5.30 measurements from mappings at four different angles are plotted. A blue reference of 0° is plotted first. After that the two large measurements of 45°(red) and 90°(yellow). The worst case for the machines as of now, 5°, is plotted in purple.

5.6.2 Analysis

After studying the result of the first test of different rotations at a 45° angle, the second test is decided to be conducted using the same orientation of the Hall effect sensors in each of the mappings. The purpose is not really to evaluate the effect of the orientation in detail as much as investigate the need to keep a consistent orientation. The right and upward orientations show very similar results though shaky at low flow rates. The downward orientation shows equally unstable behaviour at low levels, however it stabilises at a higher current for each flow. Using either left or right side orientation of the Hall effect sensor is assumed to give the same results. The result of at least one orientation that differentiates strongly from the others show a need to keep a constant orientation for reliable results.

Comparing Figure 5.28 with result from Figure 5.30 it is seen that the introduced tilt lowers the required solenoid current at each flow rate. The measurements thereby show the opposite trend compared to simulations. This indicates that a frictional force appears that reforms the force equilibrium. In Figure 5.30 a tilted sensor requires less current to hold the float at 45°, most likely because of the frictional force helps keep the float in a fixed position.

The results in Figure 5.29 have more disturbances than previous results, this also indicates that a frictional force appears. Generally in control theory, friction is modelled as a dead zone where small force deviations in equilibrium cause no resulting acceleration. Best exemplified here by the 5° measurement. The purple line shows large intervals of currents measured at the same fluid flow. The magnetic force has then been able to vary between two limits until a motion has been noticed in the float.

The 45° tilt shows a curve that is almost as stable as the one at 0°. However, the 45° and 90° tilts are not likely to occur for the sensor when mounted in a machine. The 5° tilt is most likely of the three and also the most unstable. A model for this requires a lot more theory on friction and modelling of it. An easier solution might be to suspend the sensor so that a correction for any tilt can be made.

5.7 Air Disturbance

Sometimes, air in the form of bubbles can be present in the system. It is therefore of interest to know how the new sensor behaves when bubbles are introduced. Optimal behaviour is a lower measurement, that the sensor recognizes the bubbles.

The air is inserted to the system manually by using a syringe. The injection needle is inserted through a injection valve. The injection valve is placed between the rotameter and the electromagnetic flow sensor in the system, at the red dot in Figure 5.31. To determine the amount of air to be inserted, some simple tests were conducted. Different amount of air was inserted until a noticeable difference in the volume reading was seen. The amount air decided to be used in the tests was 35 ml of air, at the pressure of the system. The air volume was inserted in pulses over a time of approximately one minute.

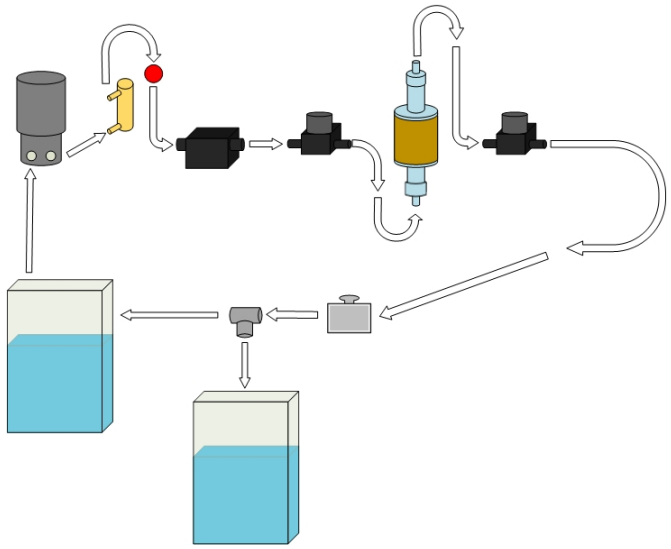

FIGURE 5.31: Red dot indicates the placement of injection valve in the test rig system.

5.7.1 Results

TABLE 5.17: Relative errors air

Sensor	*Mean [ml]*	*Standard deviation [ml]*	*Relative error comp. New sensor [‰]*
Logging without air bubbles, 350 ml/min			
Electromagnetic	700.14	0.26	0.20
Scale	705.03	0.25	7.18
Logging with air bubbles, 350 ml/min			
Electromagnetic	705.07	3.38	7.24
Scale	702.08	0.52	2.97

Table 5.17 shows results for air disturbance test. The mean value, the standard deviation and the relative error is calculated.

5.7.2 Analysis

Tests without air bubbles indicates an offset between the new sensor and the scale, due to an offset between the electromagnetic flow sensor and the scale. When tests are conducted with air bubbles, the offset decreases between the new sensor and the scale, while the mean value for the electromagnetic sensor increases.

When bubbles encounter the float, the drag force decreases and the float sinks. The position controller tries to compensate for this by also decreasing the current to the solenoid. This gives a lower flow rate measurement as the air bubbles pass. After the air bubbles have passed the float, it rises rapidly and the position controller transmits an overshoot current. This gives a higher flow rate measurement than the real flow rate. The variation of electric current affects the flow rate measurement. As seen in Table 5.17 the overshoot current contribute more to the sensor reading than the decreased current, since the offset between the new sensor and the scale decreases. The offset decreases since the new sensor measures a higher flow rate than what is actually pumped through the system.

The reason for the float passing the operating point can be the acceleration discussed regarding accuracy and precision. That the float travels a small distance between each sample. Also, the logarithmic position measurement might play a role here as well. A linearisation of the Hall effect sensor measurement might help the electromagnet increase the magnetic force earlier, when the float is rising after a bubble, and reduce the current spikes.

Studying the standard deviation of the scale for the different cases it is seen that it increases when air bubbles are introduced to the system. However, the scale standard deviation does not increases as much as the electromagnetic sensor deviation does. This indicates that the new sensor handles air bubbles better than the electromagnetic sensor.

The bubbles are inserted manually, which causes a large variation of its distribution to the system and that in turn, can effect the outcome of the results. If a large amount of air is inserted at a short time, the electromagnetic flow sensor can not measure the flow

correctly. There is also a limit for much air bubbles that can pass the float in the new sensor at one time. A large bubble or group of bubbles can lift it with such rapid force that the solenoid loses control of it and it rises to the top of the tube.

6 Discussion and Future Prospects

The discussion chapter readdresses the comparison between the conventional rotameter and the new flow sensor. Potential sources of error as well as future prospects are discussed.

6.1 Comparison Rotameter and New Sensor

In this section, a comparison is made between the conventional rotameter and the new flow sensor.

- **Fluid dynamics:** The new sensor is similar to a rotameter, when it comes to the fluid dynamics. The major difference is that a rotameter operates to keep the velocity of the fluid past the float constant. In the new sensor the velocity varies since the tube is straight, as opposed to the tapered tube of the rotameter. Reynolds number is dependent of the velocity, which means that in a rotameter Reynolds number does not change with the velocity, while it changes in the new sensor. The new principle would work with a tapered tube as well. As long as the float is held at a fixed position the velocity around it changes even if the tube is tapered or not. A straight tube is easier to manufacture, hence the manufacturing cost is reduced.

- **Pressure:** Pressure is not included in either of the two theoretical models for the new sensor and the rotameter. From the test results of the new sensor some effect due to pressure is seen. It is complex to test different pressures in a rotameter, since the reading from a rotameter is only visual. Using the different methods investigated to electrically interpret the measurement of a rotameter [2], [3] and [13] might provide more information on the effect of pressure in rotameter flow measurement.

- **Temperature:** Temperature affects the rotameter and the new sensor similarly regarding the theory and the dynamics. Changes in temperature affect the density and the viscosity of the fluid, which affects Reynolds number, the drag force and the buoyancy. The gravity force and the magnetic force are unaffected by this. The drag force and the buoyancy are affected the same way in both the rotameter and the new sensor.

- **Tilt:** When the new sensor is tilted the magnetic force still operates as it is supposed to do. A rotameter is dependent of the gravity force, which is the only counter force to the drag and buoyancy. When a rotameter is tilted the gravity force component against the flow decreases and the measurement does not function. In the new sensor the principle still works when the sensor is tilted. However, as seen in the

results, friction occurs which decreases the accuracy and the precision of the sensor. The friction also makes the sensor less reliable. If an accelerometer is implemented the new sensor might function in a tilted position, if a reliable model is created.

- **Air disturbance:** The effect of air bubbles is hard to distinguish in the case of the conventional rotameter. The air disturbances are generally quickly passing by and for the visual measurement it is solely a flicker in the float position. The bubbles can also be seen when reading the rotameter measurement and a faulty measurement is thereby recognised. For the new sensor, bubbles do affect the measurement and there is a need for some kind of disturbance protection.

The largest benefit of the new sensor, compared to a conventional rotameter, is that it transmits an electrical signal, which is easy to measure.

6.2 Sources of Possible Errors

This section discusses different possible sources of error for the tests, measurements and the design.

6.2.1 Measurement

As in all testing and measuring, calibrated instruments are a key factor to getting accurate measurements. Calibrated instruments have been used when possible. None of the calibrated instruments used were over due for recalibration. In Table 6.1 the calibrated instruments are shown with internal Baxter ID and due date for calibration. The force gauge used was calibrated during the time of the thesis but after all tests in which it was used. The force gauge passed its tests during its calibration. The general accuracy of measurements are though, as always, a possible source of error.

TABLE 6.1: Calibrated instruments used

Instrument	*Baxter ID*	*Due for recalibration*
Scale ***Mettler Toledo***	8977	8/2018
Conductivity ***Combination cond. & temp.***	4542	6/2018
Cond. probe ***paired with '4542'***	9062	6/2018
Force ***Hand held force gauge***	8717	2/2018
Pressure ***Differential gage***	8690	5/2018

6.2.2 Control

Both the pump in the test rig and the new sensor has manually tuned controllers. The pump regulator was tuned until the electromagnetic flow sensor presented a stable flow rate. Tests were later conducted when measuring the fluid flow rate with the new sensor, then the pump regulator might not be optimally tuned.

The controller for the float is tuned experimentally by changing parameters and visually observe the float. This controller is tuned until a satisfactory behaviour of the float was achieved. The optimal control parameters of the position control could be determined if more experiments and research are conducted. If the position control and measurement is optimal, the results might be more accurate and stable.

6.2.3 Methodology

In the method of mapping, the new sensors model is created with the electromagnetic flow sensor as reference. As mentioned earlier, an error in the scaling factor of volume per pulse from the electromagnetic sensor creates an offset to the real flow. Doing a fine tuning of the calibration from the provider of the sensor could create a better model.

The electromagnetic flow sensor could be used more in the logging procedure, both for controlling the flow and use as reference for target volume. The used method is more focused on attempting to measure 5000 ml with the new sensor and evaluate how well it did. The other way would be pumping a fixed volume and see how well the sensor could measure the reference volume. Apart from creating the reference volume by controlling the flow with the electromagnetic sensor, a constant, set control signal could be sent to the pump for a set time and then compare all measurements.

In the pressure tests, the pressure is set by simply turning the trim valve until a reasonable pressure is reached. The pressure variations over the time of the logging and mapping are not controlled. They are simply measured and analysed 'post hoc'. By using a method to control the pressure to remain more firmly at a level during tests, and especially during loggings, could provide better results.

In the logging procedure, the 3-way valve is opened by automation during the time the system is logging signals. The disturbance of difference in flow path and the rapid change is two things that can give a constant and a temporary error (respectively) in the measurement. The circulation path is primed when starting the system and is thereby filled with water over the whole procedures of both mapping and logging, except when testing for air disturbances. The tube leading the fluid from the 3-way valve to the scale reservoir is isolated from the other fluid until the switching of valve direction. This small volume can thereby also affect the results. Using a big target volume for the measurements can make the temporary disturbances become insignificant. The other needs to be minimized.

6.2.4 External Factors

Before the temperature control was installed a lot of drifting in the model was observed during the course of the day. Still after the introduction of the temperature controlled

reservoir, some temperature drifting was experienced when running tests at temperatures far from room temperature.

Performing tests in a climate chamber would help rule out more external factors. There has to be a discussion of how big impact the properties of ambient proximity has on the system before going to that level of controlled surroundings.

The duration of loggings can be a key parameter in test results. At high temperatures evaporation plays a bigger role. A thermally insulated reservoir helps keep the temperature constant. If the reservoir is prone to letting water vapour out, the mass might change significantly if the loggings are performed for long durations.

6.3 Future Prospects

The sensor has a few things that could be improved to get a better measurement. That will be addressed in this section. There are also a number of parameters that have not been examined in this thesis. Also, there are some parameters that needs more testing. In this section, future design and test ideas are presented, furthermore, the potential and future of the new sensor is discussed.

6.3.1 Future Designs

The design used in the tests is a result of an iterative and experimental process. To optimise the fluid dynamics, the design should be reviewed. As seen in the theory, fluid dynamics are complex. CFD analysis of the problem can help to get an optimised design of the sensor.

A thought for future design, is to create some spiral channels in the tube walls for the flow which makes the dynamics more reliable. In a gun barrel there are spiral channels in the inner wall to prompt a rotation of the bullet. The rotation of the bullet helps it keep a more stable trajectory. There is a possibility that the same improved stability could be achieved for the new sensor. It is also possible that the rotation creates a sliding bearing against the tube, which can reduce the frictional force when the sensor is tilted.

The third prototype is manufactured of transparent acrylic plastic. The plastic tube is thin and might expand at high pressures. The tube should be manufactured in a more robust material. A more robust material also allows the tube to be manufactured with higher precision.

Hall effect sensors are affected by magnetic field. If only one Hall effect sensor is used the measurement becomes sensitive to interference from magnetic fields. If two or more sensors are used to determine the position an external magnetic field affects the sensors with the same magnitude. The Hall effect sensors can be connected in a manner which ignores external magnetic fields.

From test with tilted sensor the position of the Hall effect sensors is shown to be vital. If one Hall effect sensor is used it changes its signal due to how close the float is in a radial distance. If two or more Hall effect sensors are used the radial position can be determined, and the radial position can be compensated for.

The measurement from the Hall effect sensor follows something that looks like a logarithmic function. By linearising the sensor measurement, the position control of the float could be improved. This could improve stability and measurement precision.

6.3.2 Future Testing

A limited number of tests were conducted in the thesis. To evaluate the sensor better even more tests should be conducted. Future tests could be:

- Investigate how the sensor is affected by different salinity of the liquid.
- Combining several parameters, e.g. temperature and pressure, at the same time.
- Investigate how the sensor reacts to biofilm.
- Investigate the demagnetization of the permanent magnet.
- Investigate and test more float shapes.
- Test model for the temperature.
- Experiment with different dimensions and gap size between float and tube.

6.3.3 Future of the New Sensor

The new principle shows a lot of promise under stable and well controlled conditions. Good control and measurement of temperature is a vital part of the future usage of the sensor. Whether or not it can take a place within high precision instruments is not clear, and the amount of surrounding measurement that is needed creates a few extra dimensions in complexity. The basics are still simple and given the required measurements of parameters are already present in a system, the new sensor could serve many needs of fluid measurement. Depending on properties of the solenoid and available power supply, the current measurement can be excluded by instead keeping track of the solenoids control signal.

7 Conclusion

The new principle can measure the flow rate in the range between 300 ml/min to 800 ml/min, for dialysate. The range for the new sensor is determined by its dimensions, especially the dimensions of the float and the tube. The range is also determined by the shape of the float, due to the different amount of current needed for the same flow rate.

In optimal conditions, stable temperature of the system, and correct calibration the precision is quite good. The standard deviation of the scale is 0.48 ml, when 5000 ml is to be measured at a flow rate of 350 ml/min. The offset of 37.55 ml is due to a faulty calibration in the electromagnetic flow sensor. With correct calibration a good accuracy can be achieved.

The standard deviation of the scale is lowest with 0.48 ml for flow rate of 350 ml/min, higher with 4.78 ml at 550 ml/min and highest with 22.15 ml at 750 ml/min. Results show that the precision is better for lower flows, which most likely correspond to the design of the sensor. It should be possible to plan for an optimized design from theses tests that would have good precision for the higher flow rates as well.

All tested parameters affects the measurement. The most significant changes are due to temperature. With experimental data or temperature modelling the temperature changes might be possible to compensate for. The pressure parameter has a smaller effect of the measurement than the temperature. Since the pressure is not included in any theory for the flow equation more than a slight change of density and viscosity it is believed that the pressure affects the sensor with strains, which increase the diameter of the tube. With a tilted sensor friction appears. The frictional force is difficult to predict, and causes disturbances in the measurements. With an optimal design of the sensor it might be possible to decrease the effect from a tilted sensor. Air disturbances in the system affect the measurements. The new sensor handles air disturbances better than the commercial electromagnetic flow sensor.

Theory of fluid dynamics is complex and difficult to approximate with simple equations. The approximated equations stated in the theory seems to be satisfied. The drag coefficient needs to be experimentally determined.

Applications at Baxter for the new sensor, when developed to a commercial product, can be e.g. flow control in water machines or ultrafiltration control in hemodialysis machines.

References

[1] M. Karlström and M. Pettersson F. Olsson. *Interview with Michael Pettersson*. 2018-02-20.

[2] N. Mandal et al. "Design of a Flow Transmitter Using an Improved Inductance Bridge Network and Rotameter as Sensor". In: *IEEE Transactions on Instrumentation and Measurement* 63.12 (Dec. 2014), pp. 3127–3136. ISSN: 0018-9456. DOI: 10.1109/TIM.2014.2326770.

[3] S. Sinha et al. "Design and Implementation of Real-Time Flow Measurement System Using Hall Probe Sensor and PC-Based SCADA". In: *IEEE Sensors Journal* 15.10 (Oct. 2015), pp. 5592–5600. ISSN: 1530-437X. DOI: 10.1109/JSEN.2015.2442651.

[4] C. Zhang and Y. Zeng. "New Flow Equation for Rotameter". In: *2012 Asia-Pacific Power and Energy Engineering Conference*. Mar. 2012, pp. 1–4. DOI: 10.1109/APPEEC.2012.6307015.

[5] Frank M. White. *Fluid Mechanics*. 7th ed. McGraw-Hill, 2011. ISBN: 978-007-131121-2.

[6] Lucho w2ed. *Reynolds Number*. https://commons.wikimedia.org/wiki/File:Flujo-laminar-y-turbulento.gif. Accessed: 2018-02-05.

[7] X. Zhou X. B. Zhao. *Engineering fluid mechanics*. pp 127-140. Southeast University Press, 2004.

[8] Anton Paar GmbH. *Viscosity of Water*. https://wiki.anton-paar.com/en/water/. Accessed: 2018-04-17.

[9] M. Haavisto and M. Paju. "Temperature Stability and Flux Losses Over Time in Sintered Nd-Fe-B Permanent Magnets". In: *IEEE Transactions on Magnetics* 45.12 (Dec. 2009), pp. 5277–5280. ISSN: 0018-9464. DOI: 10.1109/TMAG.2009.2023907.

[10] W. Robertson, B. Cazzolato, and A. Zander. "Axial Force Between a Thick Coil and a Cylindrical Permanent Magnet: Optimizing the Geometry of an Electromagnetic Actuator". In: *IEEE Transactions on Magnetics* 48.9 (Sept. 2012), pp. 2479–2487. ISSN: 0018-9464. DOI: 10.1109/TMAG.2012.2194789.

[11] R. Ravaud et al. "Cylindrical Magnets and Coils: Fields, Forces, and Inductances". In: *IEEE Transactions on Magnetics* 46.9 (Sept. 2010), pp. 3585–3590. ISSN: 0018-9464. DOI: 10.1109/TMAG.2010.2049026.

[12] Paul Schimpf. "A Detailed Explanation of Solenoid Force". In: 8 (Jan. 2013), pp. 7–14.

[13] N. Mandal et al. "A modified design of a flow transmitter using rotameter as a primary sensor and LVDT as a transducer". In: *Proceedings of The 2014 International Conference on Control, Instrumentation, Energy and Communication (CIEC)*. Jan. 2014, pp. 194–198. DOI: 10.1109/CIEC.2014.6959077.

[14] A. S. C. Roong, C. Shin-Homg, and M. A. B. Said. "Position control of a magnetic levitation system via a PI-PD control with feedforward compensation". In: *2017 56th Annual Conference of the Society of Instrument and Control Engineers of Japan (SICE)*. Sept. 2017, pp. 73–78. DOI: 10.23919/SICE.2017.8105536.

[15] Production-solution.com. *Coil Physical Properties Calculator*. http://production-solution.com/coil-calculator.htm. Accessed: 2018-02-19.

[16] *Speedgoat*. https://www.speedgoat.com/products-services/real-time-target-machines/baseline. Accessed: 2018-02-05.

A Magnetic Force Test

In the magnetic force test, the theory of a point of maximum force between two magnets was used [11]. By placing magnets attached to copper wires and hanging them in a force gauge at a fixed position as close as possible to the maximum point, the maximum force could be measured. There were three different magnets that were candidates for use in the floats. These primary candidates were chosen because of their cylindrical shapes which would not be able to rotate inside the float except for possibly around the lengthwise axis.

Two of magnet 1 is used in the long cone shaped float. The tests were conducted with single magnet. By experiments it was shown that adding an extra magnet increased the magnitude of the force with a factor of 1.6.

To calculate the magnetic coefficient for the equation A.1 below, the force is first multiplied with the factor 1.6 since two magnets are used. Line fitting function in Matlab is used to determine the slope of line to the data in table A.1.

C is calculated to $C = 0.3082$

$$F_m = CI \tag{A.1}$$

TABLE A.1: Results of magnetic force test 2

Current	**Magnet 1 [mN]**	**Magnet 2 [mN]**	**Magnet 3 [mN]**
0.10	30	40	150
0.12	30	40	160
0.14	30	50	190
0.16	40	60	220
0.18	40	60	230
0.20	40	70	260
0.22	50	70	290
0.24	50	80	310
0.26	60	90	350
0.28	60	100	360
0.30	70	100	380
0.32	70	110	420
0.34	70	110	430
0.36	80	110	450
0.38	80	110	480
0.40	80	120	500

B Hall Effect Sensor Test

Evaluating the Hall effect sensors sensitivity to the permanent magnets was done by applying supply voltage to one of the Hall effect sensors and then placing the magnet on pre determined distances from the sensor. The set up for the test was a rule taped to a table top. A Hall effect sensor was then placed at the zero marking of the ruler. A guide was placed along the graded edge of the ruler to create a straight track for the magnets to be moved along. From the data sheet of the sensor, an activation distance of the sensor was approximately 18 mm. This was experimentally determined to be near the maximum distance at which the sensor could detect the magnet. To have a little margin, the tests started by placing the magnet at a distance of 20 mm and then moving it 1 mm at a time. After reaching a distance of 1 mm, the measured signal did not change any further. The value of the measurement either increased or decreased depending on the direction of the magnet, i.e. what pole was directed towards the Hall effect sensor. The zero level reading was half of the supply voltage with a small offset, approx 2.53 V. In table B.1 the results of the test are presented.

TABLE B.1: Measurements of the Hall effect sensor signals for different distances to a magnet.

	Signal from the Hall effect sensor [V]	
Distance [mm]	**Direction 1**	**Direction 2**
20	2.4903	2.5520
19	2.4862	2.5560
18	2.4795	2.5630
17	2.4725	2.5718
16	2.4636	2.5790
15	2.4502	2.5918
14	2.4373	2.6042
13	2.4155	2.6243
12	2.3909	2.6500
11	2.3560	2.6783
10	2.3113	2.7329
9	2.2581	2.7727
8	2.1942	2.8549
7	2.0684	2.9624
6	1.9363	3.1056
5	1.6550	3.3712
4	1.3999	3.6412
3	0.9060	4.1030
2	0.2279	4.7950
1	0.0224	4.9645

The test with permanent magnet and current applied to the solenoid was conducted with the first prototype. The prototype was secured in a rig and current was applied with an external power supply. The permanent magnet was attached to a copper wire. The magnet was positioned at a fixed distance inside the tube of the prototype. Results from this test is seen in table B.2

TABLE B.2: Data from Hall effect sensor test with a permanent magnet when current was applied to the solenoid.

	Signal from the Hall effect sensor [V]		
Distance [mm]	**I=0.19 A**	**I=0.16 A**	**I=0.13 A**
0	2.35	2.30	2.24
1.4	2.04	1.98	1.91
5	1.32	1.26	1.19
9.9	0.72	0.67	0.60

Tests to determine the affect from he solenoid on the Hall effect sensor was conducted by applying current to the solenoid, with Hall effect sensors attached. The results is presented in figure B.3

TABLE B.3: Sensor reading from Hall effect sensor with different current applied to the solenoid.

Current [A]	**Signal from the Hall effect sensor [V]**
0.10	2.73
0.12	2.77
0.14	2.82
0.16	2.86
0.18	2.90
0.20	2.94
0.22	2.98
0.24	3.02
0.26	3.08
0.28	3.11
0.30	3.16
0.32	3.20
0.34	3.26
0.36	3.29
0.38	3.34
0.40	3.37

C Drawings

Drawings of the manufactured floats and frame.

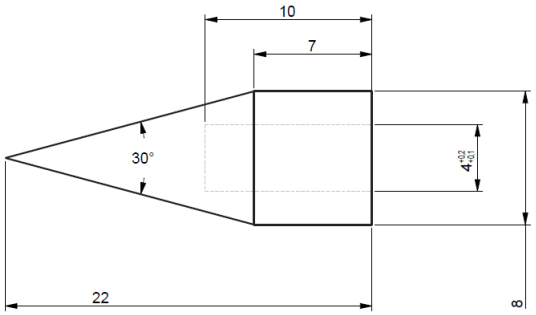

FIGURE C.1: Drawing of the cone shaped float.

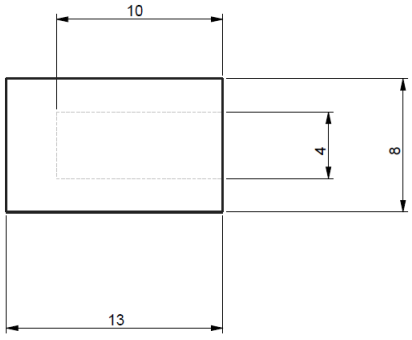

FIGURE C.2: Drawing of the cylinder shape float.

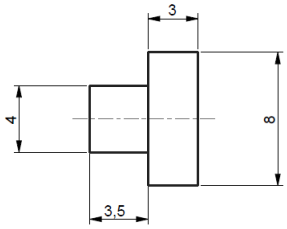

FIGURE C.3: Drawing of the lid to cover the permanent magnet inside the float

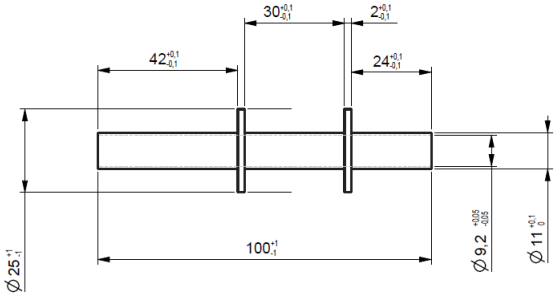

FIGURE C.4: Drawing of the frame for the third prototype.

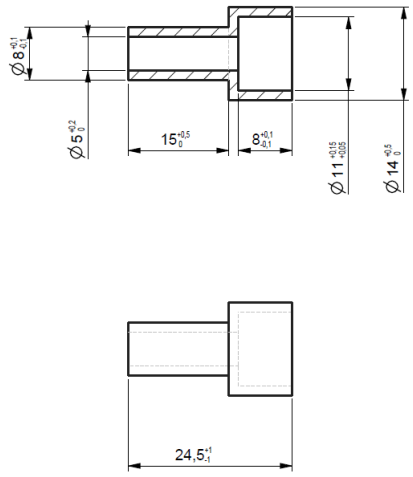

FIGURE C.5: Drawing of the tube attachments for the frame.